Investigation of natural γ–radioactivity of soil and rock samples from the Kenticha tantalite processing area of the Sidamo region

A Thesis Presented to

the School of Graduate Studies

Addis Ababa University

In partial fulfillment

of the requirements for the degree

of master of science in physics

By

Selemon Bekele

June 1995

CONTENTS

Acknowledgement

I would like to express my gratefulness to my advisor Dr. Siegfried Tesch for his valuable advice, and continual assistance throughout this work. I very much appreciate his instructive comments and suggestions which have played a crusial role in the completion of the project.

I would like to thank the school of graduate studies for the financial support I obtained to carry out the project, without which this work could not have been done.

I am greatly indepted to the department of Geology and Geophysics for providingg me with the samples to be studied by γ–ray spectroscopy. I am specially very thankful to Dr. Anatoli who had been very helpful in ssupplying the necessary information about the samples.

I extend my warmest gratitude to Ato Mulugeta Desta and Ato Zewdu Bogale of the National Scientific Equipment Centre, Science and Technology Commission, for their cooperation and help while I was working in their laboratory.

I am very thankful to the National Radiation Protection Authority and its staff for the continual help I got while working in their laboratory . My special thanks goes to Ato Hailu Woldie for his invaluable advice and support throughout my work.

I would also like to take this opportunity to thank and appreciate the ministry of education for providing me with financial support throughout my study.

Last but not least, I am quite grateful to my parents Ato Bekele Gadissa and W/o Mulunesh Mekonnen for their unrelenting help throughout all the years I have been studying.

List of figures

List of tables

Abstract

Soil and rock samples from a mining region in southern Ethiopia have been analysed for natural gamma (γ) radioactivity. A NaI(Tl) scintillation spectrometer was used to select , out of 200 samples, those with a marked level of radioactivity above the background radiation. Then a high resolution p-type germanium detector, inside a passive lead shield lined internally with copper and aluminium , coupled to a Canberra S100 MCA card was employed to measure the γ–radiation from each sample. The γ–spectra obtained were then transferred to a Canberra MicroSampo software for further analysis. The radioactivity content of the samples has been determined and the results, which may serve as baseline data for future work in environmental radiation monitoring, are discussed. The uranium and thorium activities have also been estimated so as to provide preliminary information on which type of soil and rock one should concentrate for possible prospecting of uranium and thorium minirals.

Introduction

Different kinds of radiations are extensively employed to the benefit of human beings in industry, agriculture, medicine etc.. They are also used in various research centres around the world for the advancement of science and technology. Despite their usefulness, nuclear radiations can be harmful to man and his environment. The development of the nuclear industry; the use of radiation and radioisotopes in hospitals, industry, and scientific research; the radioactivity that prevails in mining areas such as those for uranium exploration, the radiation that results from nuclear explosions and reactor accidents have made it necessary to evaluate the level of radioactivity in order to assess its impacts and implement the appropriate countermeasures to protect mankind and his environment. As a result, studies and surveys of the natural environmental radiation and radioactivity are of great importance and interest not only for general scientific reasons but also in health physics.

Natural sources of radiation make the largest contribution to the overall exposure of man through external irradiation by cosmic rays, by radioactive substances in the ground and in building materials, and through internal irradiation as a result of ingestion of naturally occurring elements in air and diet. The justification for allowing low radiation doses to the public as a result of the use of radiation and radionuclides in medicine, agriculture, industry and science should be such that the benefit always outweighs the risk of injury. The decision as to the level of exposure beyond which it is safe to use radiation is a matter of personal judgement, and by its very nature it will always be controversial. So, in the absence of conclusive data on the effects of, e.g., very low level radiation exposure, the basic reference level for the measurement of population exposure is the exposure already being incurred by man from natural sources .

Being the main source of human exposure, studies of the dose from natural radioactivity and its effects on health improve the understanding of radiation damage and, therefore, are of great value as a reference when standards and regulatory control actions are established. This requires a knowledge of what radioisotopes exist in the environment together with the amount of the radiation they emit. But radiation doses that can have serious effects on living matter are generally so low in energy terms that they cannot be detected by the physical senses of man. Thus, one has to find a means by which to detect the radiation, measure its energies and identify them with specific nuclides. One such method is gamma–ray–spectroscopy, since many of the naturally existing radionuclides are gamma emitters. So, the main objective of this work is to measure the natural gamma radioactivity of soil and rock samples, brought from Kenticha of the Sidamo region located in southern Ethiopia, using the methods of gamma–ray–spectroscopy and provide a base line data for future work in environmental radiation monitoring. In addition to this, the results obtained may provide preliminary information on which type of soil or rock one has to focus attention for a possible prospecting of uranium and thorium minerals.

In the first chapter the types of radiation that exist in the environment are briefly described. The properties of α–, β–, and γ–rays which are important from the point of view of radiation exposure to man are discussed. As the measurement of radioactivity is the starting point towards the study of radiation hazards, the second chapter deals with environmental radiation in relation to its sources, the risks associated with it, and the pathways leading to human exposure. In the third chapter the method of gamma–ray–spectroscopy for the measurement of environmental radiation is explained. The forth chapter deals with the experimental set-up for data acquisition and analysis of the results obtained.

1. TYPES OF IONISING RADIATION

1.1 Introduction

The term nuclear radiation refers to subatomic and atomic particles as well as X– and γ–rays. Natural radioactivity, nuclear reactors, accelerators and extraterrestrial sources are responsible for the existence of nuclear radiation.

When radiation is absorbed in matter, transfer of energy takes place. By transferring sufficient energy to overcome the electronic binding energy, nuclear radiation is capable of producing a separation of charge carriers or ionisation in matter. The charge separation process occurs directly or through the production of secondary radiation. Thus, the ionising radiation can be subdivided into two types: directly and indirectly ionising radiations.

Directly ionising radiation consists of charged particles, such as electrons, protons, alpha-particles, or (at high energies) of charged mesons, which ionise mostly by means of the particle–to–particle Coulomb interaction . Indirectly ionising radiations consist of uncharged species, like photons, neutrons, or uncharged mesons, which undergo interactions that release mainly energetic charged particles [ADW]. Photons and neutrons can also produce ionisation events directly during the initial interaction process. However, most of the ionisation processes are accomplished subsequent to that event by the charged particles that are released .

1.2 Natural and Induced Radioactivity

The term "Natural Radioactivity" refers to a spontaneous nuclear transition or transformation of naturally occurring unstable nuclei with the subsequent emission of radiation. The radioactivity of naturally occurring elements is related to an imbalance between the number of protons and the number of neutrons they have in their nuclei. Most elements of the periodic table have several stable isotopes. The distribution of these isotopes together with some of the longer lived naturally occurring radioactive isotopes is shown in the Segre chart, Fig. 1.1.

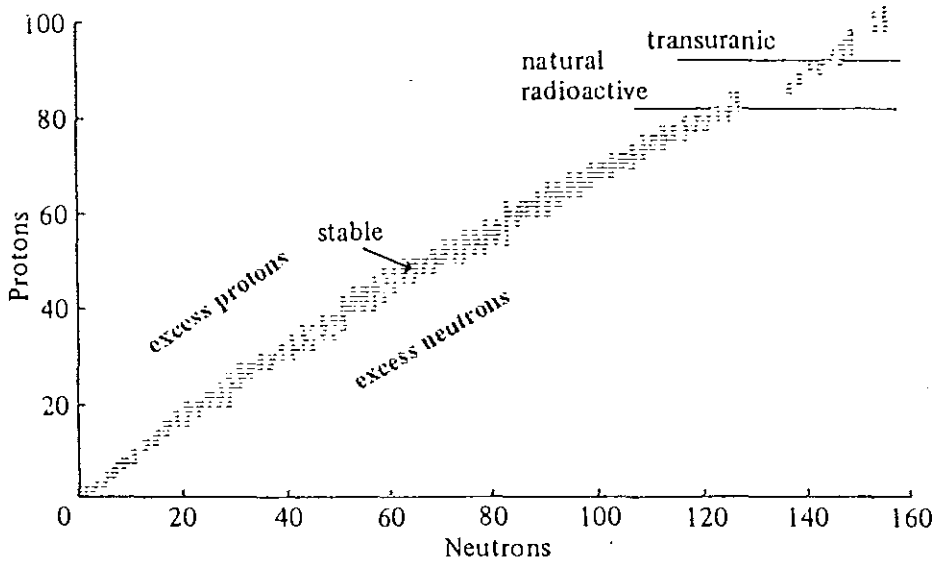

Fig. 1.1 The atomic number versus neutron number for stable isotopes and longer lived natural radioactive and transuranic elements [CPN].

Induced radioactivity is a result of bombarding naturally occurring nuclei with energetic particles such as neutrons, protons, deuterons, alpha-particles or heavy ions. Some of the artificially obtained radioactive isotopes with atomic numbers greater than that of ^{92}U, which are termed "transuranic elements", are also shown in the Segre chart [CPN].

Isotopes that do not lie within the narrow band of stability shown in Fig. 1.1. have a smaller binding energy than stable isotopes with the same charge number and will try to reach a condition of greater stability by radioactive decay. For isotopes with charge number Z greater than or equal to 82, decay occurs by the emission of either a β–particle or an α–particle or fission. In most radioactive decays the final or daughter nucleus is left in an excited state from which it decays to the ground state by the emission of γ–rays.

1.3 Properties of Nuclear Radiation

1.3.1 α – *rays*

α–rays are positively charged particles identical with doubly ionised helium atoms (He) which are emitted as a result of a decay process in which a parent nucleus transforms into a daughter nucleus and an α particle. Such a nuclear transformation can be described by the relation

$$^{A}_{Z}X \longrightarrow {}^{A-4}_{Z-2}Y + {}^{4}_{2}He + Q \qquad (1.1)$$

where X and Y stand for the parent and daughter nucleus, respectively, and Q represents the energy (Q-value) released in the process.

According to classical ideas, the minimum energy that an α–particle must have in order to escape from a nucleus should be equal to the coulomb potential barrier which is about 30 MeV in the case of uranium, and of this order of magnitude holds for most of the heavy elements. However, α–particles emitted by radioactive nuclei have kinetic energies ranging between 5 and 10 MeV. The fact that α–particles emerge out of a nucleus with

energies well below the height of the potential barrier can be explained only by the quantum mechanical tunnelling effect.

As the decay process results in only two final particles, the energy is shared uniquely between them in the inverse ratio of their masses. Consequently, a plot of the number N of α particles emitted per unit time, against their energy E consists of discrete lines indicating that alpha particles come out of the nucleus with discrete energies. For the emission to occur the value of the energy Q liberated must be positive requiring that

$$M(^{A}_{Z}X) > M(^{A-4}_{Z-2}Y + ^{4}_{2}He) \qquad (1.2)$$

where M stands for the atomic mass of the entities involved.

1.3.2 β – *rays*

For certain isotopes, another mode of decay is the emission of electrons or positrons. Isotopes which have excess neutrons over protons decay by emitting an electron together with its antineutrino. Electrons do not exist inside the nucleus but it is possible for the transformation

$$n \longrightarrow p + e^{-} + \bar{\nu}_{e} \qquad (1.3)$$

to occur within the nucleus. The proton remains in the nucleus but the electron and its antineutrino are promptly ejected, taking most of the decay energy with them. On the other hand, isotopes having an excess of protons over neutrons decay by the emission of a positron and the electron neutrino in accordance with the scheme

$$p \text{ ----->} n + e^{+} + \nu_e \tag{1.4}$$

The electrons and positrons emitted as a result of the decay processes described above are referred to as β–rays. The neutrino (antineutrino) which accompanies the emission of β–rays has no charge, and mass, if any, very small compared with that of the electron.

The β–decay process occurs between a pair of isobars, that is, two atoms with the same mass number A but different charge numbers. The charge numbers of the isobars involved in β–decay always differ by unity. The energy available for a beta disintegration is provided by the difference in mass between the initial nucleus of mass number A and atomic number Z and the sum of the masses of the final particles, that is, the nucleus of atomic number $Z \pm 1$ and mass number A and the beta particle. The disintegration energy can thus be expressed as

$$Q_{\beta^-} = \left({}^{A}_{Z}M - {}^{A}_{Z+1}M\right)c^2 \tag{1.5}$$

$$Q_{\beta^+} = \left({}^{A}_{Z}M - {}^{A}_{Z-1}M\right)c^2 - 2m_e c^2 \tag{1.6}$$

where ${}^{A}_{Z}M$ is the atomic mass of the isotope of mass number A and atomic number Z, ${}^{A}_{Z\pm1}M$ is the atomic mass of the isotope of mass number A atomic number $Z \pm 1$, and m_e is the mass of the electron. For decay to occur, the value of Q must be positive implying that

$${}^{A}_{Z}M > {}^{A}_{Z\pm1}M \text{ (} + 2m_e \text{ for positron emission),} \tag{1.7}$$

where the mass of the neutrino (antineutrino) is assumed to be zero.

The energy released in the β–decay process is shared by three particles. As a result, the β–particles can have any energy in the range from zero to the energy released in the decay process. Thus, the energy spectrum of β particles emitted by a radioactive source is a continuous one.

Some neutron deficient nuclei undergo a p ——> n conversion but have daughter products whose mass is greater than the maximum acceptable for positron emission. In such a case, the decay process proceeds by the capture of one of the orbital electrons, mostly K electrons, according to the scheme

$$p + e^- \longrightarrow n + \nu_e \qquad (1.8)$$

and the process is referred to as "electron capture". The decay by electron capture yields the same daughter nucleus that would have been produced by positron emission, had this been energetically possible.

Following electron capture there will be an orbital vacancy, usually in the K–shell, and this will be promptly filled by an electron from one of the outer orbitals accompanied by the emission of the characteristic X–ray of the daughter element. Alternatively, the energy available for each of the X–rays may be transferred to one of the orbital electrons which will be ejected from the atom. Electrons so ejected as an alternative to X–ray emission are called Auger electrons.

1.3.3 γ – *rays*

After undergoing a nuclear decay process, the nucleus is often left in an excited state. The nucleus tends to relieve the excitation by the emission of γ–rays which are electromagnetic quanta of energy in the range of about 10 keV to several MeV, with their corresponding wavelengths lying between 10^{-10} to 10^{-12} m. The mean life time of an excited nuclear state before de-excitation usually ranges from about 10^{-14} to 10^{-10} seconds. There are however, a number of known cases where a nucleus can exist in an excited state for a long time. Nuclei of this type are called isomers and their corresponding nuclear states are called isomeric or metastable states. γ–radiation from a metastable state leads by what is known as "Isomeric Transition" (IT) to the ground state. In this type of transition, only the energy content of the nucleus is changed.

Since nuclear transitions occur only between discrete energy levels, the γ–ray spectrum from any radionuclide consists of discrete lines.

As an alternative to γ emission, an excited nucleus in some cases may return to the ground state by giving up its excitation energy to one of the orbital electrons around it, which is ejected from the atom. This process is referred to as "Internal Conversion" as the γ–ray is not emitted but can be thought of as being converted to kinetic energy of the electron emitted. Tables of internal conversion coefficients can be found, e.g., in ref. [DHG].

1.4 Natural Radioactivity in Soil and Rock

A study of the radioactivity from soil and rock is important not only in terms of environmental monitoring but also for getting information about undiscovered mineral resources like uranium and thorium . This knowledge is important for establishing an energy policy, in guiding the direction of exploration, and can aid in focusing exploration on areas best suited for further discoveries of reserves. In particular, the localisation of uranium concentrates is helpful in identifying favourable areas in terms of mineral resources because uranium, thorium and other natural radiation sources are commonly associated with other elements, and significant correlations with Be, Va, Cu ,Ni ,Nb, Ga, Rb and others have been found [IAEA8]. As a result, the earth sciences were among the first where nuclear techniques have been applied and a lot of experience has been accumulated in employing nuclear techniques in the exploration and exploitation of energy and mineral resources, as demonstrated in an IAEA symposium in 1990 [IAEA9]. Among the various applications we mention:-

- nucleonic control systems and on-stream analysis in the coal industry
- on-line nuclear analytical techniques in the mineral industry
- on-stream analysis of ore concentrations
- nuclear bore-hole logging
- environmental protection, on-line monitoring of pollutant traces, determination of changes of the background radiation caused by mining activities etc. .

It should also be stressed that nuclear techniques in fundamental and applied research are of great importance in that nuclear science research has provided powerful tools to monitor the environment and preserve the integrity of the ecosystem [IAEA10]. This aspect is particularly important for the energy and mineral industries as they release CO_2, H_2S, NO_x

dust containing heavy metals into the atmosphere and waste water with heavy metals into rivers and lakes resulting in contamination of the environment .

Already in the first years of the 20th century many discoveries of the radioactive properties of the chemical elements were made . However, these investigations became crucial after man-made radioactivity from nuclear power plants, from fuel reprocessing, from nuclear explosions, reactor accidents etc. prevailed . As this work is aimed at investigating natural γ–radioactivity of soil and rock samples brought from the Sidamo region, a brief outline of the main radioactive sources in the earth's crust is given in the following paragraphs .

Much of the natural radioactivity around us comes from primordial nuclides in the earth's crust having half-lives comparable to the age of the earth. Soon after the discovery of radioactivity, about 20 single primordial radionuclides, most of which are beta or alpha emitters with half-lives between about 10^{10} to 10^{17} years, were detected (e. g. ^{50}V, ^{113} Cd, ^{147}Sm, ^{204}Pb, ^{40}K, ^{87} Rb). Apart from ^{40}K and ^{87}Rb, the rest exist in small concentrations.

^{40}K is found in all living things independent of the fact that the isotopic abundance is very small (0.012%). With a branching ratio of 11% ^{40}K undergoes β^+ decay to the first excited state of ^{40}Ar, and a gamma ray with energy of 1.460 MeV appears. The other branch (89%) of the ^{40}K instability is the β^- decay to the ground state of ^{40}Ca with an end point energy of 1.33 MeV. The other singly occurring radioactive nuclide is ^{87}Rb with an abundance of 27.8%. It undergoes beta decay to ^{87}Sr directly to the ground state with an end point energy of 274 keV.

On the other hand, four chains of radionuclides are known to exist . These can be described in terms of their mass number A as

$$A = 4m + n \tag{1.9}$$

where m is the largest integer divisible by A and n is the remainder. As heavy nuclei undergo mostly beta or alpha decay, the four possible types of nuclides are within the 4m, 4m + 1, 4m + 2, 4m + 3 series. Three of the chains are found in nature due to the fact that the leading radionuclides have half-lives long compared to the age of the earth. The fourth series 4m+1 or neptunium series starts with ^{241}Pu (half-life 13.2 years) which decays to ^{241}Am by the emission of a β–particle. Because of their shorter half-life compared to the age of the earth, all daughter nuclei in this series are not found in nature. After a sequence of alternate β– and α–decays, all the three naturally found series end up with a stable isotope of lead . The 4m or thorium series, starting with ^{232}Th, ends up with ^{208}Pb having an abundance 51.55%. The 4m+2 or uranium series finishes with ^{206}Pb whose abundance is 26.26%. The 4m + 3 or actinium series stops at ^{207}Pb with an abundance of 20.8%.

Tables of the uranium, thorium, and actinium series are given in appendix A. The radioisotopes ^{220}Rn, ^{226}Ra, and ^{222}Rn which are important in relation to natural radiation exposure of man are discussed in detail in the next chapter.

2. ENVIRONMENTAL RADIATION MONITORING

The increase in the number of nuclear reactors for power production, the widespread use of nuclear radiation and radionuclides in medicine for diagnosis and treatment of diseases, agricultural and industrial uses of radioactive materials, the fact that natural background radiation is the major contributor to human exposure, all make it necessary to find ways to deal with the possible hazards of nuclear radiation . As a result, the potential effects of ionising radiation on human population have been a concern of the scientific community for several decades and the establishment of the International Commission on Radiological Protection (ICRP) in 1928 was a result of such concerns [IAR]. The ICRP has maintained continuing studies of radiation protection problems that are of special importance to the radiation control programme of many nations.

2.1 Sources of Radiation in the Environment

The various types of radiation that exist in the environment come from natural sources, fission products, and activation products. The natural sources of radiation are classified into

(a) external sources of extraterrestrial origin,

(b) radiation of terrestrial origin, and

(c) internal sources, consisting of the naturally occurring radionuclides that are taken into the body.

Even though this work is concerned mainly with the measurement of natural radioactivity in soils and rocks, it is worth describing in a brief manner the above mentioned sources so as to have an insight into their impact on man and the environment. The various sources of radiation in the environment are displayed in Fig. 2.1.

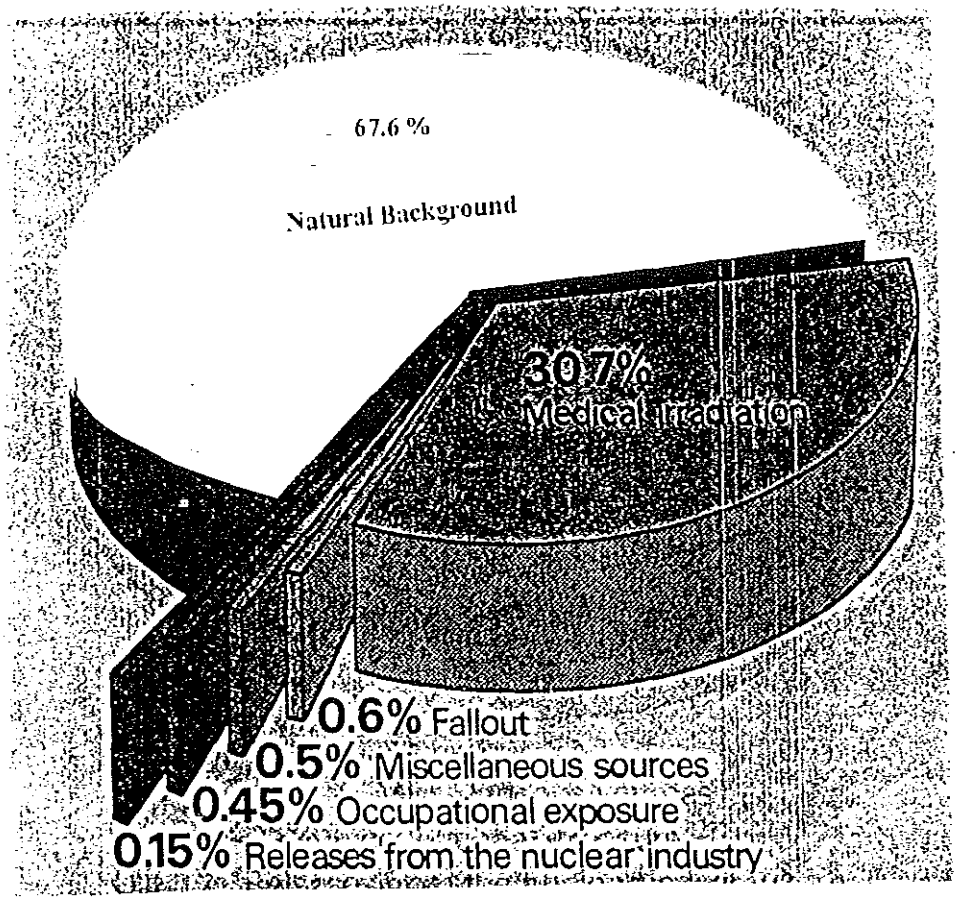

Fig. 2.1 A schematic diagram illustrating the relative contribution of various sources to environmental radiation [IAEA11].

The primary cosmic radiation, which originates in outer space and impinges on the top of the atmosphere, consists of 79% protons, 20% alpha particles, about 0.7% carbon, nitrogen and oxygen nuclei, and about 0.22% nuclei of atomic number greater than 10. The interactions of these primary particles with atmospheric nuclei produce electrons, nucleons, pions and gamma rays. At sea level the muons from pion decay account for about 80% of the cosmic radiation and electrons about 20%. The important radionuclides, from the stand point of radiation monitoring, resulting from this interaction are tritium (^{3}H), ^{14}C, and ^{7}Be. Of lesser importance are ^{10}Be, ^{22}Na, ^{32}P, $^{33P, 35S}$ and ^{39}Cl [EIM]. Radiation of terrestrial origin

comes from the primordial radionuclides ^{40}K, ^{87}Rb, and those in the uranium and thorium and actinium series [IAEA3].

The primary sources of radionuclides produced in the fission process are atmospheric testing of nuclear weapons and releases from nuclear facilities as a result of accidents or of removal wastes. Large explosions in the atmosphere (now forbidden) disperse most of the radioactive material into the stratosphere, where it stays for some time and depending on the altitude and latitude of the test site, the mean retention time is estimated to be from less than a year to about five years [IAEA1]. Fallout can therefore occur years after an explosion has injected material into the atmosphere. Smaller detonations carry the radioactive material only into the troposphere, and fallout occurs within days or weeks. Fission products were also reported to have been present after accidents like the Chernobyl nuclear power plant accident. The dominant fission products are mainly the radionuclides ^{90}Sr (half-life 28 years), ^{137}Cs (half-life 30 years), and some γ emitting radionuclides from tropospheric fallout, e.g., ^{95}Zr and ^{106}Ru.

Activation products are mainly produced during nuclear power production. The nuclear fuel cycle includes several steps: mining and milling of uranium ores, enrichment of the isotopic content of ^{235}U for some types of reactors, fabrication of fuel elements, production of energy in the reactors, reprocessing of irradiated fuel and recycling the fissile and fertile nuclides recovered, transportation of nuclear materials between fuel cycle installations, and finally disposal of radioactive wastes. Although most of the radioactive materials associated with nuclear power production are present in the irradiated fuel, small amounts are released into the environment in effluents at each of the steps in the cycle described above. In addition to fission products, neutron activation gives rise to radioactive

components in structural and cladding materials. Activation products discharged to the atmosphere as a result of waste disposal, accidents and the likes include the transuranic elements and the hydrogen radioisotope (^3H), activation gases containing carbon, nitrogen, sulphur, argon, caesium, cobalt, iron, manganese, zinc, iodine and a host of other radionuclides [IAEA1].

2.2 Pathways in the Environment

The series of ways or chains which lead to the ultimate radiation exposure of man are referred to as "pathways". In order to make a satisfactory assessment of the impact radiation exposure has on man, and hence take the necessary steps to protect him against the dreadful consequences and carry out a careful monitoring of his environment, one has to be thoroughly aware of the various paths that nuclear radiations follow to finally reach man. The main exposure pathways in the environment are illustrated in Fig. 2.2 .

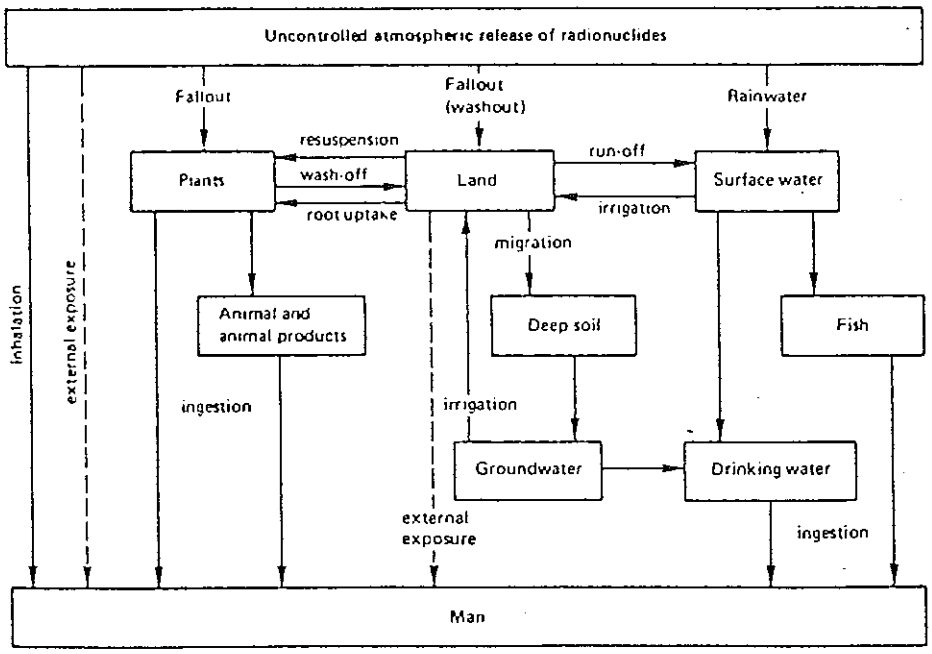

Fig. 2.2 Exposure pathways in the environment [IAEA3].

The natural (or background) radiation from outer space contributes to the contamination of the environment through the interaction of cosmic rays with atmospheric constituents resulting in radioactive nuclei which could be inhaled directly from the air or ingested if deposited on vegetables and cereals that man uses for food. Uptake of deposited nuclides on soil and the natural radionuclides of the earth by plants, crops etc. through their roots also leads to the exposure of man as a result of ingestion, but direct exposure to gamma rays is possible too.

The radionuclides due to fallout either from atmospheric testing of nuclear weapons or accidents at certain nuclear facilities may contaminate the environment through deposition on:-

- agricultural areas the produce of which consumed both by man and domestic animals will give rise to internal radiation doses and, in addition, all living organisms in the area (man, animals and plants) will be subject to external radiation;
- grazing pastures where cattle get the major part of their diet (meat and milk obtained from animals feeding on contaminated pastures is one of the ways for internal exposure through ingestion);
- bodies of water like rivers, lakes, etc. for drinking and irrigation purposes. In addition, the contamination of fish, edible seaweed, algae etc. constitutes a significant pathway in the exposure of man to nuclear radiations [IAEA2].

2.3 The Risks of Ionising Radiation

The interaction of radiation with human tissue, at any level of exposure, involves the risk of initiating a serious disease such as cancer or leukaemia, or producing detrimental genetic effects which may appear in future generations. The nature and severity of these biological

effects and the time at which they show up depend on how much radiation is absorbed and the rate at which it is received. Radiation injuries can be divided into two classes: somatic effects in which the damage occurs in the irradiated individual himself, and hereditary effects which arise only in the offspring of the irradiated person as a result of radiation damage to germ cells in the reproductive organs. In order to gain an insight as to why environmental monitoring is necessary, it is essential to look into some examples that can somehow illustrate the risks of nuclear radiation. In the following paragraphs are discussed some of the hazards which result from uncontrolled radiation exposures [SJR].

The ingestion of radium and other radionuclides which are similar to calcium in their chemical properties causes bone cancer as a result of the continual irradiation of the bone into which such substances have been incorporated. Such cases were witnessed during the first quarter of this century among individuals who were exposed to radium being used in luminous dial manufacturing and in luminous paints and among patients who received radium for medical purposes. Strontium and plutonium have also similar properties to radium and therefore are potential hazards to man if they are present in his environment.

The high incidence of lung cancer among miners has been attributed to the presence of high concentration of radon gas in the atmosphere of the mines. However, the ability of the lung to concentrate particulates increases the relative risk of inhaling radioactive substances in the form of aerosols compared to the risk of inhaling a radioactive gas. As a result, although radon contributes to the total exposure to a small extent, the principal dose is due to its daughter products which tend to accumulate in the lung. By this mechanism the daughter products contribute about 20 times as much dose as does the radon.

Exposure of the eye lens to X–rays, γ–rays, β–particles and neutrons may result in the development of cataracts which have been observed among survivors of the Japanese bombings during the second world war, among patients whose eyes were treated by X–, γ– or β–rays, and among a few employees who were exposed to radiation at accelerators [EIM].

Leukaemia has been observed to occur among Japanese survivors at Hiroshima and Nagasaki, among children irradiated with X–rays during their infancy for the treatment of enlarged thymus, among patients treated with ^{131}I for problems of hyperthyroid and with X–rays for cancer of the cervix, and among physicians exposed in the practice of radiology. X–ray irradiation of children and adults for the treatment of enlarged thymus and adenintis may also lead to the development of thyroid cancer.

2.4 Environmental Radiation Monitoring

In any modern society, any course of action that may produce a risk to the public has to be accompanied by a monitoring program in order to check the correct performance of the operations and to evaluate the relevant risks for the public.In the nuclear field, environmental monitoring may be defined as all the surveys, measurements, investigations and assessments carried out on man and his environment which are capable of meeting the conditions mentioned above [IAEA5].

In environmental radiation monitoring, the prime objective is to evaluate all the parameters causing radiation exposure to man, to estimate the population dose and recommend measures to keep radiation exposure to a minimum. To meet the objectives of radiation

protection, the ICRP [IAR], recommended the following requirements concerning all sources of nuclear radiation:-

Justification: no practice resulting in human exposure to radiation should be authorised unless its introduction produces a positive net effect, even taking account of the resulting radiation detriment;

Optimisation: all exposures should be kept "as low as reasonably achievable", taking into account the relevant social and economic considerations;

Individual dose limitation: the dose equivalent to individuals from all practices (save those specifically excluded) should be less than the appropriate dose limits.

Regarding the natural background radiation, the main interest lies in monitoring of ^{222}Rn and ^{220}Rn which are among the first of the natural radioactive nuclides discovered at the beginning of this century. ^{226}Ra in the uranium series decays to radon that disintegrates to a polonium isotope (^{218}Po) which by further decay through isotopes of lead, bismuth, and polonium ends with a stable isotope of lead (^{206}Pb). ^{220}Rn is produced by the decay of ^{224}Ra in the thorium series and decays by α–particle emission to ^{216}Po which decays through isotopes of thallium, lead, bismuth and polonium to a stable isotope of lead (^{208}Pb).

Since they occur in nature, man has always been exposed to a large extent through inhalation of their decay products. The major source of exposure consists of radon and its decay products emanating from the ground and from building materials found in domestic housing. In some countries the radiation dose to man caused by inhaled radon daughters constitutes more than 50% of the total radiation dose from other natural or artificial sources. Extensive measurements of ^{222}Rn, ^{220}Rn and their decay products in the domestic

environment to determine their concentration have been measured in many countries around the world [USB].

^{222}Rn also poses a big problem in the nuclear fuel cycle because it gives rise to an occupational exposure during uranium and thorium mining and is a source of exposure to the public during storage of waste (tailings) from the milling of the mills. The radiation risks in underground uranium mines are primarily from the airborne radionuclides consisting of ^{222}Rn and its short lived daughters whose concentrations are usually higher in underground mines than in the open pit types. ^{222}Rn is an inert gas and it passes freely into, and out of the lungs with a minimal uptake by the respiratory system and presents no grave danger. On the other hand, the radon daughters ^{218}Po, ^{214}Pb, ^{214}Bi, and ^{214}Po are often attached to dust particles and condensation nuclei in the air so that they are significant from a radiation protection point of view. The airborne dust also contains long-lived radionuclides from the ^{238}U and ^{235}U series as a result of mining operations such as drilling and blasting. In the mills, the long-lived alpha emitters in the form of dust are usually more significant than radon and its daughters.

The radionuclides ^{238}U, ^{234}U, ^{230}Th, ^{226}Ra, ^{210}Po, and ^{210}Pb are significant from the viewpoint of internal irradiation and for the purposes of radiation protection while β– and γ–radiation emitted from the radionuclides in the ore is mainly responsible for the external radiation risk in mines. In the open pit uranium mines the air born radiation risk is much less important than in underground mines. This is the result of natural ventilation, which will dilute the radon gas and radon daughter concentrations in the atmosphere. The major sources of radiation risk in the open pit mines are external radiation and radioactive dust containing the long-lived radionuclides.

In the case of thorium mines, thorium production is mostly through processing of mineral sand mined by the open pit methods and, as a result, the radiological risk, particularly from inhalation may be small compared to underground mining. In underground thorium mines or in uranium mines where thorium is present in significant quantities, the radiation risk occurs due to ^{220}Rn daughters and external radiation. Thus the assessment of risk includes an assessment of thorium and its long-lived daughters in the working atmosphere in addition to ^{220}Rn and its daughters. External radiation risks arise from both beta and gamma radiation emitted by ^{228}Ra, ^{228}Ac, ^{228}Th, ^{224}Ra, ^{212}Bi, and ^{208}Tl [IAEA1].

3. METHODS OF GAMMA RAY SPECTROSCOPY

^{222}Rn and ^{220}Rn are chemically inert, noble gases and they occur in almost all materials and for the most part (90% or more) are trapped in the solids carrying their precursors ^{226}Ra and ^{224}Ra [USB]. Accordingly, the measurement of the gamma radiation emitted from the materials provides an indication of its uranium and thorium content as most of the gamma radiation from the ^{238}U and ^{232}Th series arises from the ^{222}Rn and ^{220}Rn progeny. So the problem in determining environmental radioactivity reduces to the simple matter of identification of several components in a complex mixture of radionuclides and measuring their concentration. Most of the naturally existing radionuclides are γ–emitters The method of gamma-ray-spectroscopy (GRS) can be applied for such purposes since a mixture of many different gamma emitting isotopes even at low concentration levels can be analysed simultaneously with no preparation necessary except volume reduction of the environmental samples to achieve the optimum geometry for counting [IAEA6].

The technique of gamma-ray-spectroscopy involves the measurement of the energy and intensity of gamma radiation whereby individual γ–rays can be identified with specific elements, and the intensity of each γ–ray provides a direct measure of the element abundance. In GRS the interaction of γ–rays within a detector results in the conversion of energy into signal pulses which can be collected by applying a potential difference across the detector. The pulses produced in the detector are usually very small and must be amplified for further processing such as counting and pulse height analysis. For pulse amplification and pulse height analysis an electronic circuit is employed while a computer is used for data processing and evaluation.

3.1 Interaction of Gamma Rays with Detector Materials

The interaction of gamma rays with matter is primarily through three mechanisms, namely, the photoelectric effect, the Compton scattering, and pair production depending on their energy. There are a number of other mechanisms also, certain of which can be of importance in special cases.

In the photoelectric effect it appears that a photon interacts with the atom of a medium as a whole. The energy of the photon is transferred to an electron, usually to the one in the innermost shells, which is ejected out with a kinetic energy

$$E_{kin} = h\nu - E_b \tag{3.1}$$

where E_b is the binding energy of the orbital electron. When the vacant electron shell thus left is refilled, one or more characteristic X-rays are emitted. The photoelectric effect is stronger for lower energy gamma-rays and for absorber materials of high atomic number and the probability of the photoelectric interaction occurring is approximately [DHG] given by

$$\tau = const. \frac{Z^{4.5}}{E_\gamma^3} \tag{3.2}$$

where Z is the atomic number of the absorber and E_γ is the energy of the interacting photon. The strong dependence of the interaction cross-section on the photon energy is the reason why this effect is the dominant type of interaction at low energies, but becomes negligible at high energies.

In Compton scattering the primary photon may interact with any one of the orbital electrons. The electrons are considered essentially as free electrons under the condition that

the primary photon energy is large compared with the electron binding energy. The interaction is an elastic collision between the primary photon and the electron. The energy is shared between the recoil electron and the secondary photon. Except for very low incident energies, the angular distribution of the scattered γ–rays is strongly forward peaked. Two extreme values are important in Compton scattering. The first is the minimum energy of the scattered γ–ray that occurs at a scattering angle of 180^0. This minimum energy of the backscattered γ–ray is 255.5 keV. The second extreme value of interest is the energy of the electron recoiling at 0^0, termed the Compton edge energy. This forward scattered electron accompanies the 180^0 backscattered gamma-ray since there can be no transverse component of momentum in this case. For γ–ray energies in the region of 1 MeV the difference is about 0.2 MeV. The probability of the Compton scattering [ADW] is given by

$$\sigma = \pi r_o^2 \left\{ \frac{2(1+\alpha)}{\alpha^2} \left(\frac{2(1+\alpha)}{1+2\alpha} - \frac{\ln(1+2\alpha)}{\alpha} \right) + \frac{\ln(1+2\alpha)}{\alpha} - \frac{2(1+3\alpha)}{(1+2\alpha)^2} \right\} \qquad (3.3)$$

where r_o = classical radius of the electron, $\alpha = h\nu/m_o c^2$, and m_o is mass of the electron. The cross-section or probability expression for high energies can be obtained from eq. (3.3) in the limit where $h\nu >> m_o c^2$, i.e., $\alpha >> 1$:

$$\sigma = \pi r_o^2 \left(\frac{1 + 2\ln 2\alpha}{2\alpha} \right) \qquad (3.4$$

From eq. (3.4), it can be seen that the probability of the Compton effect varies as the inverse power of the primary photon energy .

In pair production the primary photon disappears in the vicinity of a nucleus or an electron, and its energy goes to the rest mass and the kinetic energy of the positron-electron pair which is produced.. This process can only take place in the neighbourhood of a nucleus (Occasionally, but rarely, in the electric field of some other charged particle) to make conservation of momentum possible. The threshold energy for pair production [ADW] is given by

$$h\nu_{min} = 2m_e c^2\left(1 + \frac{2m_e c^2}{2Mc^2}\right) \qquad (3.5)$$

where m_e is the mass of the electron and M can be the mass of a nucleus or an electron depending with which particle the photon interacts. When a nucleus is involved, eq. (3.5) gives $2m_ec^2 = 1.022MeV$ for the threshold energy since $M >> m_e$ and if an atomic electron is involved, $m_e = M$ and the threshold energy is $4m_ec^2 = 2.044MeV$. One should remember that even though the pair production process mainly takes place near a nucleus, it is extranuclear; the particles produced are not nuclear emissions. The probability of the pair production process varies with Z^2 and dominates at higher energies .

3.2 Detection of Gamma Rays

All methods of detection of charged particles, uncharged particles like neutrons, or electromagnetic radiation depend on their interaction with the matter they pass through. When radiation interacts with matter, it induces reactions such as ionisation, excitation,, fission or activation. The operation of different detectors depends on the resultant effect of one of these processes, and as a result, radiation detectors are constructed of materials which can easily be ionised, excited, or get activated etc..

Several of the oldest and most widely used types of radiation detectors are based on the effects produced when a charged particle passes through a gas. The primary modes of interaction involve ionisation and excitation of the gas molecules along the particle track. The electron–ion pairs thus created result in electrical signals that can be detected by means of an associated electronic circuit. Ionisation chambers, proportional counters, and GM–tubes are examples of detectors that make use of gas as the interaction medium.

Another class of detectors known as scintillation counters consist of materials which emit light when they are exposed to radiation. The scintillation process essentially involves the formation of excited electronic state of atoms or molecules and the emission as light of the absorbed energy when the atom or molecule returns to its ground state. Certain organic and inorganic crystals, liquid and solid organic compounds and gases can be used as scintillators. Examples of organic scintillators are Anthracene, Stilbene, while NaI(Tl), ZnS(Ag) belong to inorganic scintillators. The high Z value of the constituents and high density of inorganic crystals favours their choice for γ–ray spectroscopy, whereas organic scintillators are often preferred for beta and fast neutron spectroscopy [PWJ].

A third class of detectors contains semiconductor materials like silicon or germanium. When radiation passes through a semiconductor, the overall significant effect is the production of electron-hole pairs which constitute electric signals that, under the action of an applied electric field, is collected by the appropriate electronic circuit.

3.2.1 Ionising Effects of Nuclear Radiation

A nuclear radiation gives rise to ionisation when it passes through gaseous, liquid or solid matter. The amount of energy lost by the radiation whether it consists of charged particles

or gamma quanta must exceed the ionisation potential of the atom of the stopping material or the energy needed to excite an electron-hole pair in a solid such as a semiconductor. An approximate value for the average energy needed to create an ionisation in gas is 35 eV. On the other hand, an expenditure of 3.6 eV on the average is required to produce an electron-hole pair in silicon whose energy gap is 1.1 eV. In germanium, whose energy gap is 0.7 eV, only about 3.0 eV is needed to create an electron-hole pair [CPN].

3.2.2 Energy resolution and detection efficiency

The important characteristics of any detector material are its energy resolution and detection efficiency. Energy resolution is a measure of a detector's ability to distinguish closely spaced energy lines in a spectrum corresponding to a given radiation. A quantity that characterises the energy resolution is the full width at half maximum (FWHM). The energy resolution of a detector is conventionally defined as the FWHM divided by the location of the peak centroid, and therefore, is a dimensionless fraction usually expressed as a percentage, except for semiconductor detectors and ionisation chambers in which case the FWHM is given in energy units of eV, keV, etc..

There are a number of potential sources of fluctuation in the response of a detector which gives rise to imperfect energy resolution. These include any drift of the operating characteristics of the detector during the course of the measurements, sources of random noise within the detector and the instrumentation system, and statistical noise arising from the discrete nature of the measured signal itself. The third source is in some sense the most important because it represents an irreducible minimum amount of fluctuation that will always be present in the detector signal no matter how perfect the remainder of the system is made.

The statistical noise arises from the fact that the charge Q generated within the detector by a quantum of radiation is not a continuous variable but instead represents a discrete number of charge carriers. By assuming that the formation of charge carriers follows a Poisson process, an estimate can be made of the amount of inherent fluctuation. Under this assumption, the resolution R of a detector [KGF] is given by the equation

$$R = \frac{FWHM}{H_O} = \frac{2.35\sigma}{kN} = \frac{2.35}{\sqrt{N}} \tag{3.6}$$

for scintillation detectors, and

$$R = FWHM \qquad (in\ eV,\ keV\ etc.) \tag{3.7}$$

for semiconductor detectors and ionisation chambers, where FWHM = 2.35σ, $H_0 = kN$ is the peak centroid, $\sigma = kN^{1/2}$ is the standard deviation, k is a proportionality constant, and N is the number of charge carriers. However, careful measurements of the energy resolution of some types of radiation detectors have shown that the achievable values for R can be lower by a factor as large as 3 or 4 than the minimum predicted by the Poisson statistics. In order to characterise the departure of the observed statistical fluctuations in the number of charge carriers from the pure Poisson statistics, the so-called "Fano factor" (F), which is defined as

$$F = \frac{observed\ \ variance\ \ in\ \ N}{Poisson\ \ predicted\ \ variance\ in\ N} \tag{3.8}$$

is introduced. In terms of the Fano factor, the resolution is expressed [KGF] as

$$R = 2.35\sqrt{\frac{F}{N}} \tag{3.9}$$

Any other source of fluctuation in the signal chain will combine with the inherent statistical fluctuations from the detector to give the overall energy resolution of the measuring system. If each source of fluctuation is independent, the total FWHM will be the square root of the quadrature sum of the FWHM values for each individual source:

$$(\mathrm{FWHM})^2_{\mathrm{overall}} = (\mathrm{FWHM})^2_{\mathrm{stat}} + (\mathrm{FWHM})^2_{\mathrm{noise}} + (\mathrm{FWHM})^2_{\mathrm{drift}} + \ldots \tag{3.10}$$

Detection efficiency relates the number of pulses counted to the number of photons incident on a detector. Counting efficiencies are divided into two classes: absolute efficiency and intrinsic efficiency. The absolute efficiency is defined as

$$\epsilon_{abs} = \frac{number\ \ of\ pulses\ \ recorded}{number\ \ of\ radiation\ \ quanta\ \ emitted\ by\ source} \tag{3.11}$$

and are dependent not only the on detector properties but also on the details of the counting geometry. The intrinsic efficiency is defined as

$$\epsilon_{int} = \frac{number\ \ of\ pulses\ recorded}{number\ \ of\ quanta\ \ incident\ on\ \ detector} \tag{3.12}$$

and no longer includes the solid angle subtended by the detector as an implicit factor. For isotropic sources the two efficiencies are related by

$$\epsilon_{int} = \epsilon_{abs} \frac{4\pi}{\Omega} \tag{3.13}$$

where Ω is the solid angle subtended by the detector at the location of the source. The intrinsic efficiency usually depends primarily on the detector material, the radiation energy,

and the physical thickness of the detector in the direction of the incident radiation. The overall efficiency of a detector is equal to the product of a number of factors, and is expressed as

$$\epsilon_d = f_g f_{bs} f_{sa} f_a \epsilon_{int} \quad (3.14)$$

where f_g is the geometry factor, f_{bs} is the backscatter factor, f_{sa} is the self absorption factor, f_a is the absorption factor of the intervening medium [BGR].

3.2.3 Sodium iodide [NaI(Tl)] scintillation detectors

Before the advent of semiconductor detectors the NaI(Tl) scintillation detector was the mainstay of modern gamma ray spectroscopy. A crystal of pure sodium iodide is not suitable for use as a scintillator. When an ionising radiation passes through the crystal it causes electrons in the valence band to jump across the forbidden gap to the conduction band. Upon returning to the valence band, these excited electrons recombine with the holes left behind thereby emitting quanta of light in the ultraviolet region of the spectrum.

As the energy of the light given off is the same as the energy gap, most of the light will suffer self absorption within the crystal. In addition, the glass window in front of the photo-multiplier strongly absorbs light of wave length around 200 nm. Even though, the self absorbed light may again excite electrons from the valence band to the conduction band, returning to the valence band is possible for the electrons without the emission of radiation as a result of radiationless transitions. The overall effect of the above processes is that the number of quanta escaping from the scintillator will be small. So, in order to obtain visible light from the crystal, a few percent of an impurity called the activator is included in the solution from which the crystal is grown. This impurities create intermediate energy levels within the forbidden gap so that electrons from the conduction band can break their return

at these intermediate levels and so emit quanta of light of lower energy and longer wave length given by

$$\lambda = \frac{1224}{\Delta E} nm \qquad (3.15)$$

where ΔE is the spacing between the energy levels of the activator. The advantageous properties of the NaI(Tl) detector over gas filled ones are its relatively good resolution (e.g. a line width, FWHM of about 7% or 45 keV at a γ–ray energy of 622 keV), the good physical and chemical stability of the crystal and its relatively high efficiency [SKA].

3.2.4 Germanium detectors

In order to serve as a suitable radiation detector, a semiconductor must have as large an intrinsic region as possible where incident radiation effectively produces electron-hole pairs. The high purity germanium detector which is a semiconductor device having a PIN structure serves this purpose. It is fabricated [HKH] from a germanium crystal in which the impurity concentration is reduced to about 10^{10} atoms/cm^3 so that the corresponding resistivity is sufficiently high and a depletion depth of about 10 mm can be reached using a reverse bias of less than 1000 volts.

The advantage of HpGe detector over the NaI(Tl) scintillator is that it has a very high resolving power. Its shortcoming concerning detection efficiency can be overcome by using relatively larger sizes even though the cost of production is much higher. The justification lies in the large amount of information that can be obtained in the analysis of complex spectra by using such detectors .

3.3 Electronics and Data Acquisition System

In modern gamma ray spectroscopy the electronics and data acquisition system consists of a detector bias supply, preamplifier, amplifier, multi-channel analyser (MCA), a data storage device and a display for monitoring the progress of a measurement. A schematic diagram of a modern gamma ray spectroscopy system is shown in Fig. 3.1, and the main elements of this system are described in the following sections.

3.3.1 Detector bias supply

In order to collect the charges formed in the detector, a bias voltage must be applied across the detector. This voltage is chosen low enough to avoid breakdown or arcing, but otherwise as high as is safe since the charge collection process improves with increasing voltage. The bias voltage must be stable in order to maintain the same voltage gradients in the detector and thereby the same charge collection characteristics. The optimum bias voltage for a given detector is generally specified by the manufacturer and could be from a few hundred volts for a small detector to over 4 kV for a large one depending on the detector material itself.

3.3.2 Preamplifier

A preamplifier serves a dual purpose. Firstly, it amplifies the small detector pulses by about 10^2 for semiconductor and gas-filled detectors, but only by unity for scintillation detectors. Secondly, by providing a match between the high impedance of the detector and the low impedance of the cable to the amplifier it overcomes signal attenuation when it is required to drive a signal into a long cable which leads to the main amplifier with only a negligible loss of amplitude. The preamplifier is usually located close to the detector to reduce the capacitance of the leads which can degrade the rise time and lower the effective signal size.

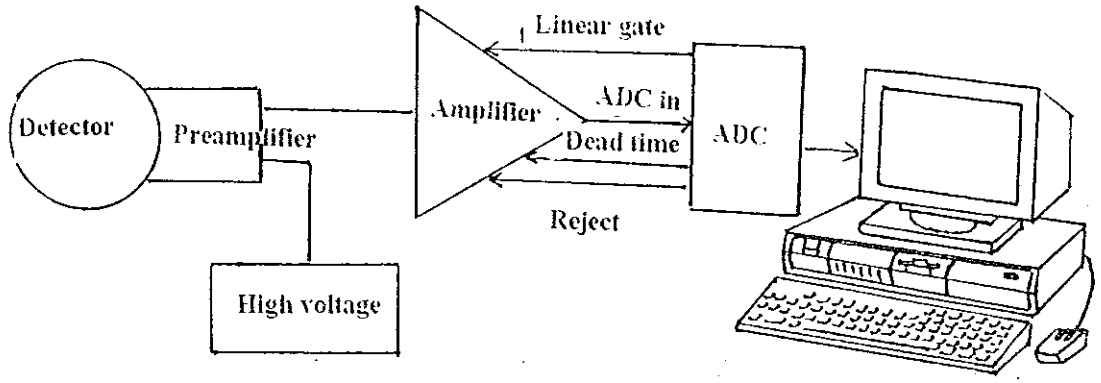

Fig. 3.1 A Schematic diagram of a modern γ–ray spectroscopy system.

3.3.3 Amplifier

The heart of any spectroscopy system is the amplifier. For energy spectroscopy, the primary purpose of the amplifier is to magnify the amplitude of the pulses from the preamplifier from the mV range into the 0.1 to 10 V range. This is done by using the gain controls of the amplifier.

Often, the requirement to handle high counting rates is in conflict with the need for optimum energy resolution. Achieving the optimum energy resolution requires long pulse widths, that is, the best energy resolution for the peaks in a spectrum will be obtained with longer time constants since the system can then average the noise over a longer time. On the other hand, short pulse widths are essential for high counting rates in order to minimise pile-up effects. As a result, a compromise pulse width must be chosen which optimises the quality of information to be obtained. This is done through the use of controls that enable one to select the appropriate shaping time constants of the amplifier used.

At ordinary counting rates, the step rise caused by each detector event rides on the exponential decay of a previous event, and the preamplifier output does not get the chance to return to the base line. Since the amplitude of detector events is usually variable and the time of event occurrence is random, the preamplifier output is irregular as shown in Fig. 3.2. To overcome this problem, the amplifier shapes the pulses to optimise energy resolution and to minimise the risk of overlap between successive pulses. In addition to this, most amplifiers incorporate a base-line restoring mechanism to insure that the base line between pulses is held rigidly at the same level.

As a result of the long exponential decay on the preamplifier output pulse, there is a noticeable undershoot (overshoot) as the amplifier pulse attempts to return to the base line. At medium to high counting rates, a large fraction of the preamplifier output pulses will fall on the undershoot (overshoot) from a previous pulse. Consequently, the apparent pulse amplitudes measured for these pulses will be too low (high), which leads to a broadening of the peaks recorded in the spectrum. It is therefore essential that amplifiers incorporate a mechanism to eliminate the problems associated with the presence of these undershoot (overshoot) effects. This is achieved through the use of the so-called pole-zero cancellation method whose benefit is improved peak shapes and better energy resolution.

When two or more gamma rays arrive at the detector within the width of the spectroscopic amplifier output pulse, their respective amplifier pulses pile up to form an output pulse of destorted amplitude. So, to avoid the difficulties which result from pile-up events, the amplifier implement a method known as pile-up rejection to prevent the analysis of such unwanted events. Fig. 3.3 shows how the use of a pile-up rejecter (PUR) improves the resolution of a measuring system.

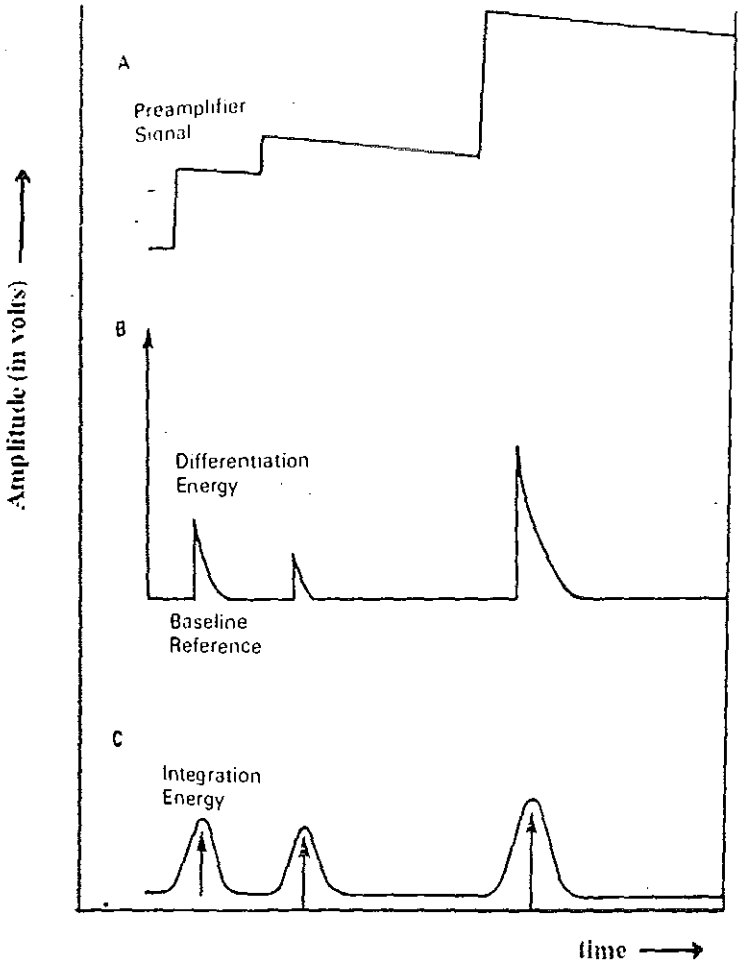

Fig. 3.2 Signal pulses from a) preamplifier, b) amplifier after base line restoration, c) amplifier after pulse shaping [CNP].

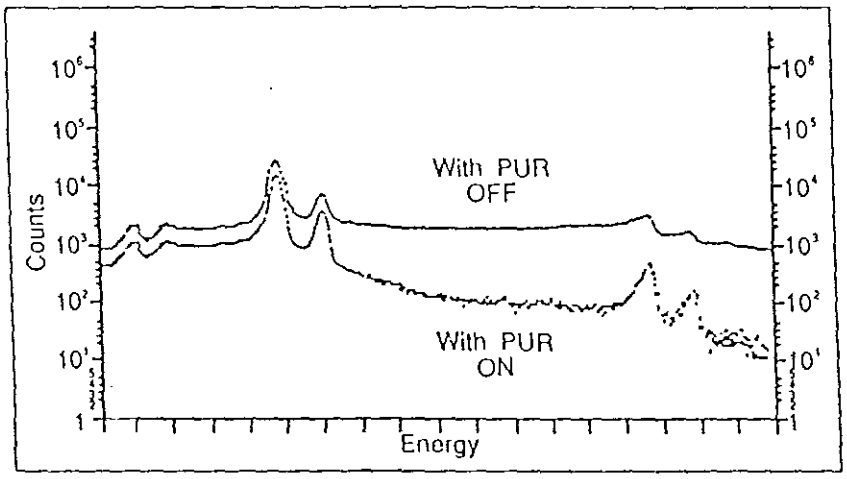

Fig. 3.3 Spectrum of a ^{57}Co source taken without and with pile-up rejection [CNP].

3.3.4 Multi-channel analyser (MCA)

The basic task in any spectrometry is the measurement of the pulse-height distribution at the amplifier output. The data acquisition is accomplished by means of a single channel analyser (SCA) or a multi-channel analyser (MCA). The single channel analyser has lower and upper discriminator levels, and produces an output logic pulse when the input pulse lies between the discriminator levels. With this device all voltage pulses in a specific range can be selected and counted. An additional SCA can be added for a second voltage range, and so on. The single channel analyser can be used for pulse height measurements but one has to gradually search through the pulse height distribution by setting the discriminator to a narrow voltage range and going through a range of voltages since in this case only pulses whose amplitudes fall between two pre-set limits will produce the desired output. This process is time consuming, particularly when high energy resolution is needed in the spectrum, because when examining one pulse height range all the remaining information has to be rejected. A way out of the difficulty mentioned above is to employ a multi-channel analyser which can examine each pulse height and store information about the number of pulses within narrow ranges of pulse height. A pulse range of, e.g., 0-8 Volts can be divided into 256, 512,1024, up to 16 k numbers of equal pulse height intervals that are called channels. The heart of such a device is the analog-to-digital converter (ADC) that measures the maximum amplitude of an analog pulse and converts that value to a digital number which is a proportional representation of the analog signal. This number is then used to select an address in a memory bank and the address contents are then incremented by one to record that pulse. In this way, sequentially arriving pulses can be sorted out and stored in the corresponding channels according to their heights. A live display of the pulse height spectrum being collected is provided via a video monitor and

the memory contents (the spectrum) to a printer, or to a graph plotter, or disk recorder or to a computer for further analysis [CNP].

3.4 Background Interference in γ-Ray Measurements

In carrying out gamma-ray spectroscopy measurements, it is essential to minimise background interference from various sources. The background radiation comes from cosmic radiation, from the natural primordial radioisotopes like ^{238}U, ^{232}Th, and ^{40}K in the earth's surface and in building materials, from the materials of construction of the associated detector equipment, and from the sample being counted particularly if it contains nuclides emitting high-energy gamma rays.

The contributions from the primordial nuclides present in the vicinity of the detector can be effectively reduced by making use of shielding materials. The material given preference for such a purpose is lead because of its large Z number and high density usually in the form of bricks or interlocking cylinders stacked so as to enclose the detector. Although shields 10 cm thick are common, a leading shield of 5 cm is sufficient for most experiments. The contribution of cosmic rays to the background cannot not be reduced to the same extent, on the contrary, it may even increase, since the number of cosmic ray interactions resulting in secondary high-energy radiation is proportional to the mass of the shield.

A further source of background radiation is X–ray fluorescence which is produced as a result of γ–rays which happen to interact with the atomic electrons within the shielding material . Since for some measurements the energies of this radiation may interfere with those of the photons under study, the internal walls of the shield must be lined with a material capable of absorbing the X–rays. In the case of lead, the X–ray energies are around

80 keV (K_α X–rays) and 12 keV (L_α X–rays). To absorb these X–rays a sheet of cadmium 1 mm thick can be used as the cladding material. Further lining with a 0.2 mm copper sheet will almost completely absorb the cadmium X–rays.

Radioactive impurities in the shielding material may give rise to additional background . For example, lead is known to contain ^{210}Pb (46.5 keV gamma rays) and its daughter ^{210}Bi (beta rays of 1161 keV maximum energy leading to Bremsstrahlung). It may also contain man-made contaminants like ^{60}Co and ^{137}Cs . Thus, especially in low-level measurements, it is important to use low-background materials. The equipment ancillary to the detector should also be made of very low background materials to make their contribution to the overall background as small as possible.

If the sample being counted has a high content of high-energy gamma emitting nuclides, the Compton background will dominate the environmental background. Massive shielding will do nothing to improve the sensitivity of the system for low energy gamma-rays in the presence of relatively higher energy radiation. In such cases, the so-called Compton suppression method can be employed to reduce this background. The Compton continuum is primarily caused by gamma rays which sustain one or more collisions and scatter out of the germanium detector without imparting their full energy leading to concealment of low activity peaks. The Compton suppression spectrometer usually consists of a Ge detector surrounded by NaI(Tl) or plastic scintillation guard detectors a simple version of which is shown in Fig. 3.4. The electronics system is arranged to turn off data acquisition whenever a photon escapes the germanium detector and is seen by one of the guard detectors. In this way, only those events attributed to gamma rays which have dissipated their full energy

within the Ge detector are analysed by the MCA [IAEA4]. Fig. 3.5 shows gamma spectra without and with a Compton suppression.

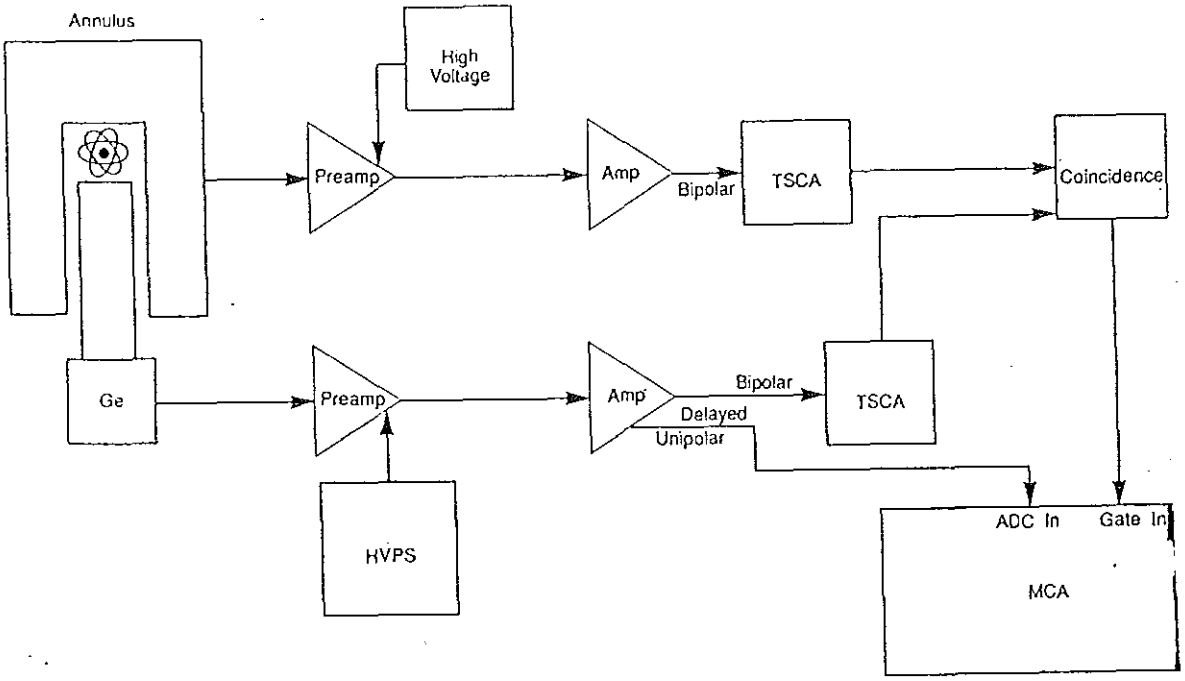

Fig. 3.4 γ–ray spectrometer with Compton suppression system. TSCA stands for timing single channel analyser [CNP].

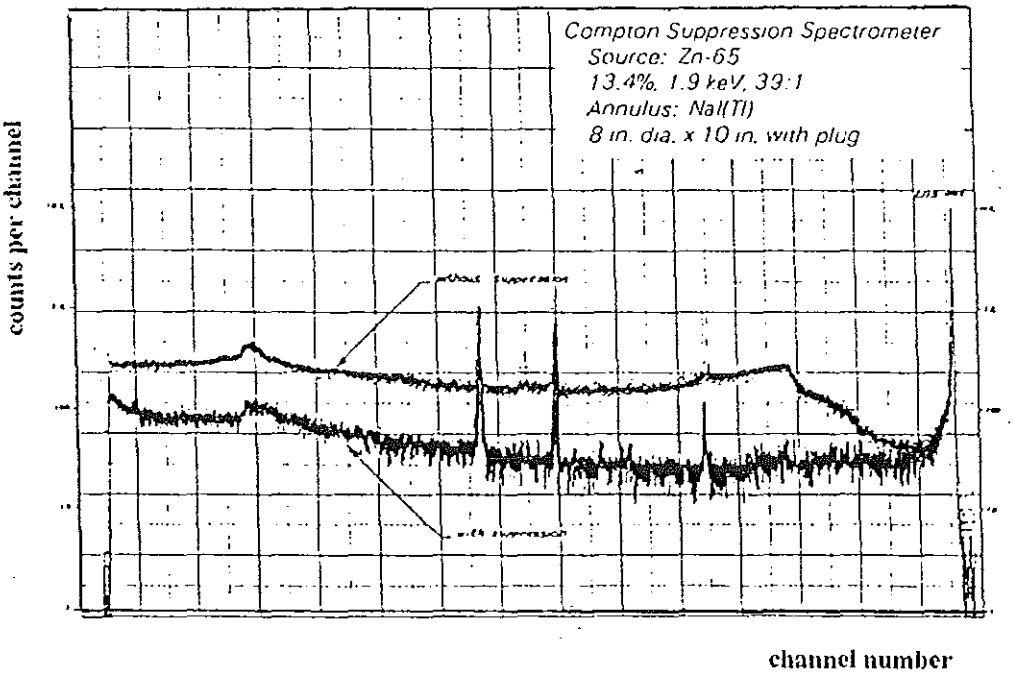

Fig. 3.5 γ–ray spectrum of ^{65}Zn obtained with and without Compton suppression [CNP].

4. DATA ACQUISITION AND ANALYSIS

4.1 Geological Features

The Adola area is a mining region located to the south of Ethiopia where gold and tantalite concentrates are being produced at a large scale. In order to illustrate the main geological features of the place a schematic geological map of it is presented in Fig. 4.1. The region is characterised by metamorphic rocks of the basement complex intruded by acidic, basic and ultrabasic igneous rocks of Gariboro ultrametamorphic intrusive complex, Adola magmatic series, root-tectonic quartz, quartz bearing Gabbro-voritos, granites and pegmatites.

The rocks of the basement are subdivided into two complexes: the middle complex and the upper complex . The middle complex is represented by the metamorphic rocks of Bore Buluka, Zembaba, Aflata and Kenticha formations, while the rocks of upper complex are characterised by the Chakata, Finkilcha formations and Kajimiti beds .

In addition to the intensive metamorphic events, the rocks have gone through complicated folding and faulting processes which together have led to the present structural features of the area.

The Kenticha region is characterised by rare-metal (tantalite)-bearing pegmatite [EAF] ores which are found within the south-eastern part of the region shown as the area enclosed by the dashed lines in Fig. 4.1, which is referred to as the rare-metal bearing belt . The rocks of the Kenticha formation are widely distributed within the belt. They are folded, faulted and intruded by ultrabasic rocks and granitic bodies in relation to which the late complex rare-metal-bearing pegmatites have been formed.

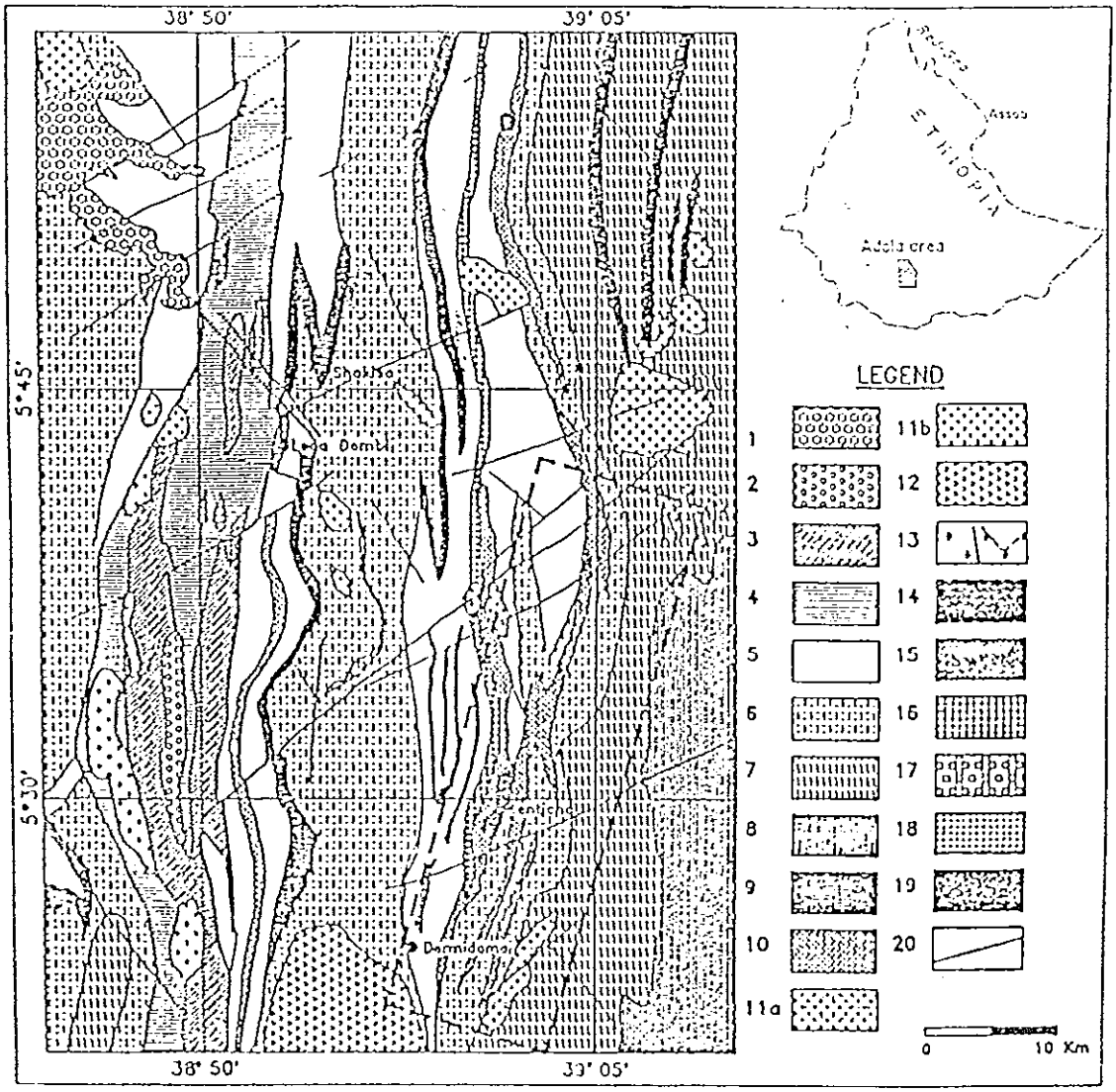

Fig. 4.1 Geological map of the Adola area (MODIFIED FROM E.M.R.D.C., 1981)

1. Recent basalt, 2. Kajimiti beds; 3. Finkilcha formation; 4. Chakata formation; 5. Kenticha formation; 6. Aflata formation; 7. Zembaba formation; 8. Buluka formation; 9. Amphibolite;10. Tolo-chlorite-tremolite schists; 11a. Two-mica granites; 11b. Biotite granite; 12. Gariboro massif with granite gneisses and migmatites; 13. Sub volcanic intrusions; 14. Serpentinites; 15. Micaschists; 16. Gabbro; 17. Kyanite schists; 18. Graphite schists; 19. Marbles; 20. Fault.

4.2 Sampling Techniques

Two hundred samples were collected from different locations throughout the rare metal bearing belt of the Adola gold field. The sampling sites, which were randomly selected, are shown in Fig. 4.2. The initial weight of all samples collected was in the range 1.8-2.0 kg. The dotted trench and aerial chip methods of sampling were employed for sample collection. To obtain representative materials for laboratory investigations, the samples were further reduced in size to less than 10 mm by crushing . After successive mixing by the cone and circle method and reduction by quartering, the initial weights of the samples were reduced to fall in the range 0.225 – 0.250 kg. The flow sheet describing the process mentioned above is given in appendix B. For the measurement with the NaI(Tl) spectrometer no further sample preparation, apart from taking part of the material which could easily be put in a suitable container, was carried out since the aim in the first stage of the work had been to select those samples showing remarkable radioactivity. For the measurements with the high-purity germanium detector, each selected sample was ground with mortar and pestle, and passed through a 1 mm sieve mesh . All the samples were then put into cylindrical containers with screw capes.

4.3 Measurement with the NaI(Tl) Detector

In order to gain experience on how to use scintillation detectors for the measurement of radioactivity and to screen out those samples which exhibit a marked level of radioactivity a NaI(Tl) crystal of 5 cm x 5 cm encased in an aluminium can with entrance window 0.5 mm (density 147.9 mg/cm^2) the inside part of which is covered with a reflecting oxide 1.6 mm thick and density 88 mg/cm^2, and provided with magnetic shield (in order to avoid the deflection of the electrons moving within the photomultiplier tube) was used. The detector had an energy resolution of 7.5% to 8.5% at 662 keV of ^{137}Cs and was surrounded by a

passive shield in the form of lead bricks 5 cm thickness stacked one upon the other. The electronics system consisted of a Canberra manufactured model 2007 preamplifier, model 2024 amplifier, and a model 8075 ADC with an S100 MCA. In order to make the full range of 4k channels correspond to an energy interval from 0 to 1500 keV, the electronics system was set as given in table 4.1.

Table 4.1 Setting of the electronics system for the NaI(Tl) detector

Bias Voltage	Amplifier	ADC	MCA
980 V	Coarse gain 30	Gain 4K	Range 4K
	Fine gain 0.48	Range 4K	
	Shaping time 4μs	Offset All Zero	

With the above setting maintained throughout the measurement, the background without shielding was measured for an hour and then, with the detector surrounded by lead bricks as shown in Fig. 4.3, the background measurement was repeated for three hours. The spectra obtained are depicted in Fig. 4.4. As can be seen there is a marked interference from the surrounding especially at lower energies where bremsstrahlung from interaction of secondary cosmic rays like protons, electrons etc. dominates. The effect of using a shield is apparent from Fig. 4.4b. A reduction of the background by a factor of about 25 has been obtained. A representative portion of each sample was then put in a plastic container of diameter 6 cm and height 1.5 cm. As the aim was to select the samples with discernible activities above the background, seventeen samples out of two hundred were chosen on the basis of the total integrated counts for further measurement with a germanium detector. The spectrum for the highly active sample, KL, is shown in Fig . 4.5.

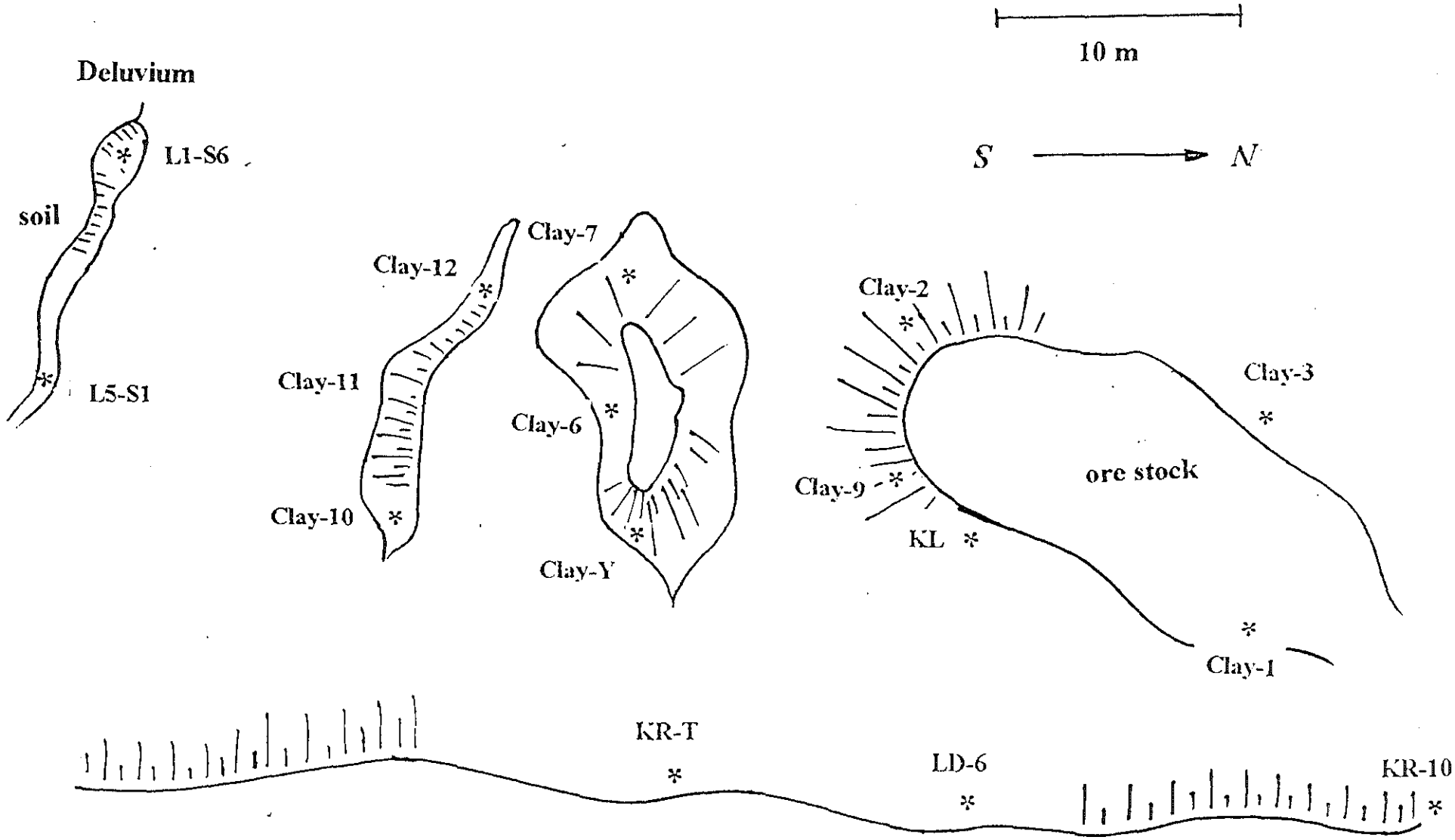

Fig. 4.2 Arial view of the sites for the samples selected for measurement with the HpGe detector.

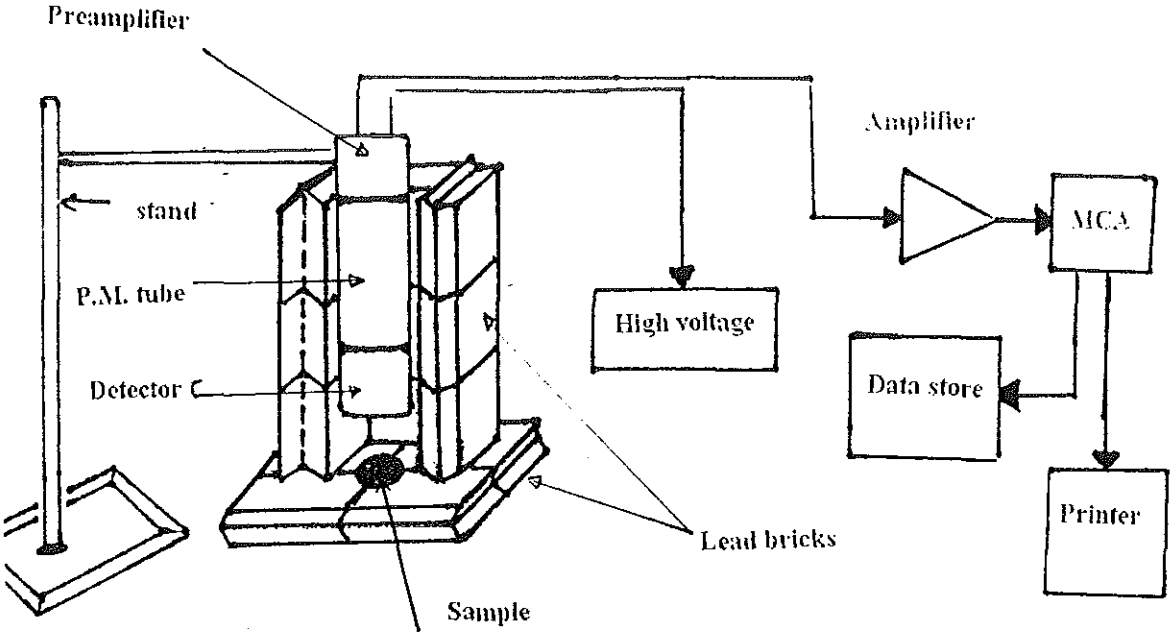

Fig. 4.3 Schematic diagram of the NaI(Tl) measuring system.

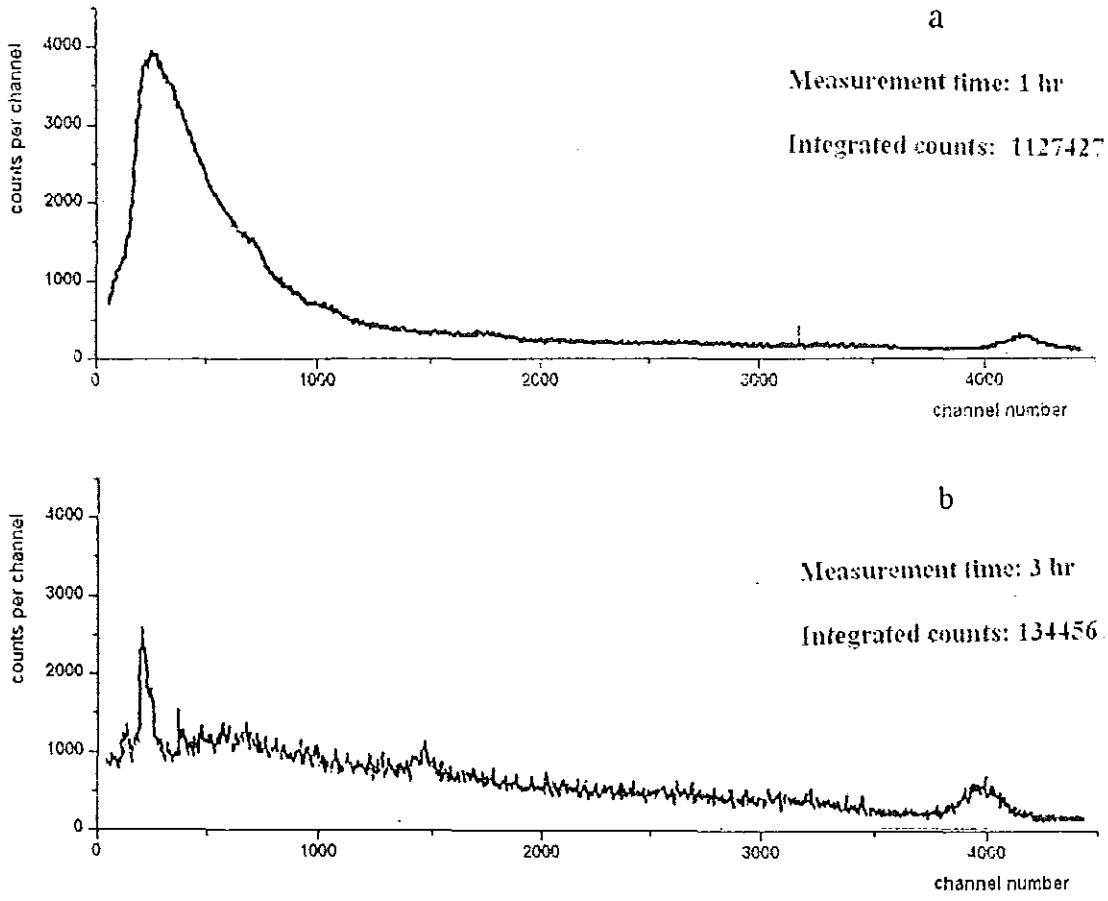

Fig. 4.4 Background spectrum as measured by the NaI(Tl) detector: a) without shielding b) with shielding.

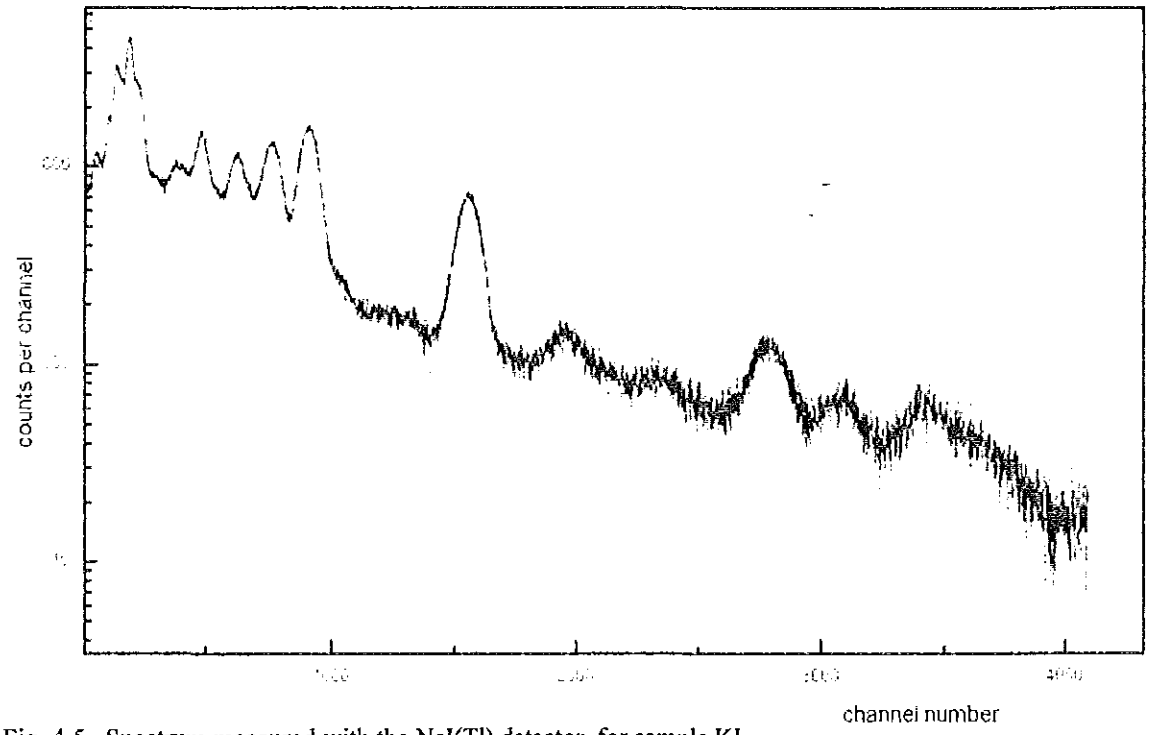

Fig. 4.5 Spectrum measured with the NaI(Tl) detector for sample KL.

4.4 Measurement with the HpGe Detector

The gamma spectroscopy system consisted of a coaxial high purity germanium (HpGe) detector of diameter 48 mm, length 34.5 mm , active area 18.1 cm^2 inside an aluminium can, with 5 mm distance from window, surrounded by a cylindrical lead shielding of thickness 10 cm. The detector provides an efficiency of 13.7 % at 1.33 MeV relative to a 7.62 cm x 7.62 cm NaI(Tl) scintillator at a source to detector distance of 25 cm. The resolution at the same energy is 1.75 keV FWHM with a peak to Compton ratio of 44.3:1. A schematic diagram of the detector configuration is shown in Fig.4.6.

After being ground with mortar and pestle and passed through a 1 mm sieve, the samples were put into cylindrical containers of diameter 9.4 cm and height 4 cm. Samples C2, C11, C12, and LD6 filled to a height of 2 cm, 3 cm, 3.2 cm, and 1.8 cm respectively. The remaining samples each filled to a height of 4 cm. Each sample was placed on top of the

detector and all the samples were counted for eight hours in order to minimise the inherent statistical errors, with the electronics system set as given in table 4.2.

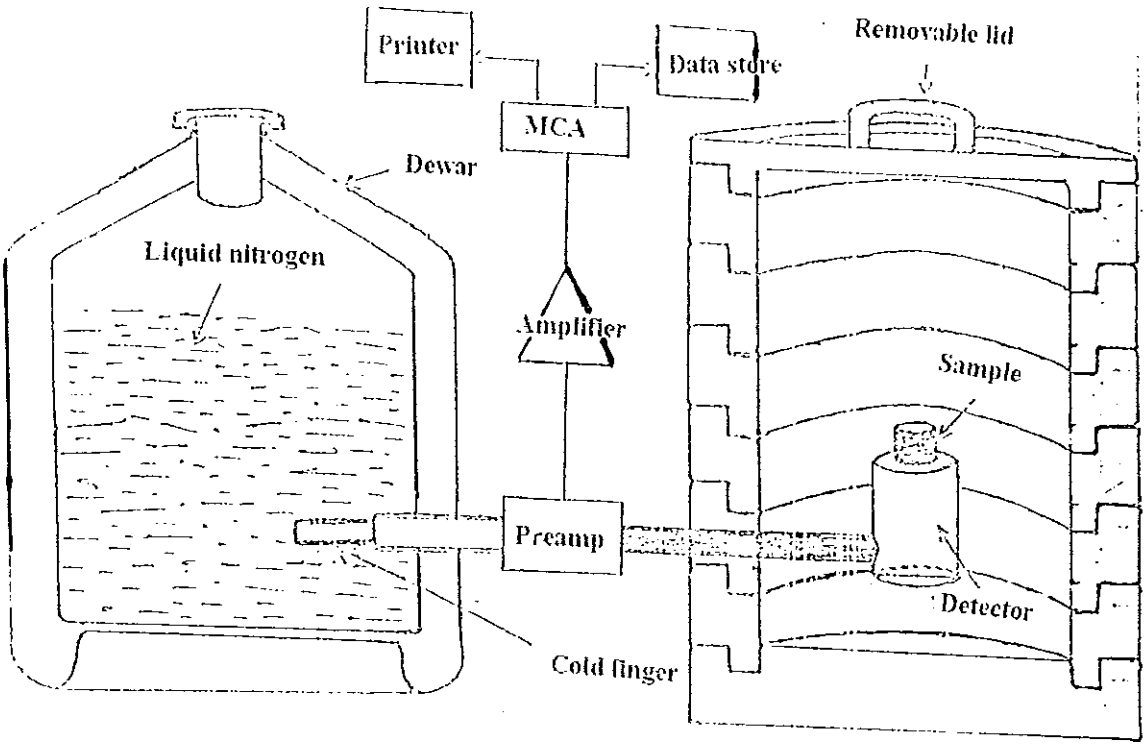

Fig .4.6 Schematic diagram of the HpGe measuring system.

Table 4.2 Setting of the electronics system for the HpGe detector

Bias voltage (model 3105)	Amplifier (model 2021)	ADC (model 8075)	MCA
4000 V	Coarse gain 30	Gain 4K	Range 4K
	Fine gain 0.36		
	Shaping time 4μs	Range 4K	
	PUR Off		

The big difference between the resolutions of the HpGe and the NaI(Tl) detectors can be seen from Fig. 4.7. This is as expected since a quantum of photon produces more

information carriers in the HpGe detector than in the NaI(Tl) detector for the same amount of energy lost, and a large number of charge carriers means better resolution.

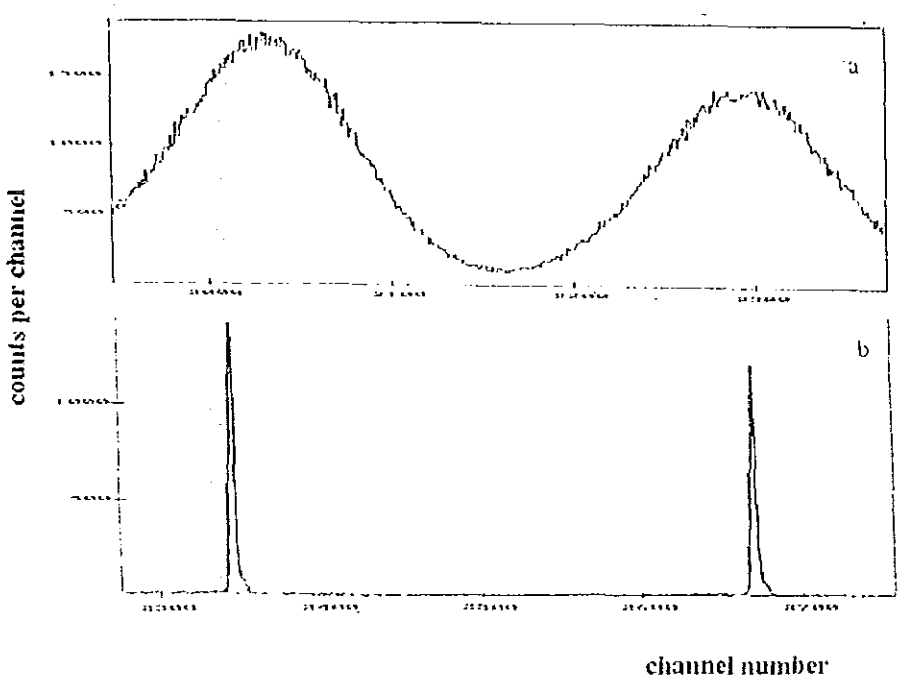

Fig. (4.7) Spectra for a ^{60}Co source measured with a) NaI(Tl) detector , b) HpGe detector.

Making use of standard point sources for energy calibration, a relation was established between energy values and channel numbers by a least squares fitting procedure which resulted in the straight line depicted in Fig. 4.8. The flow chart of the MicroSAMPO software used for the energy calibration and further analysis of the measured spectra is given in appendix C. The sources and their energies used for the calibration are given in table 4.3.

Table 4.3 Values of channel numbers (C) and energies (E) used for energy calibration

C	124	521	575	683	739	1,188	1,304	1,577	2,344	2,550	2,668	2,928
E(keV)	81	276.4	302.9	356	383.9	604.7	661.7	795.8	1,173.2	1,274.5	1,332.5	1,460.8

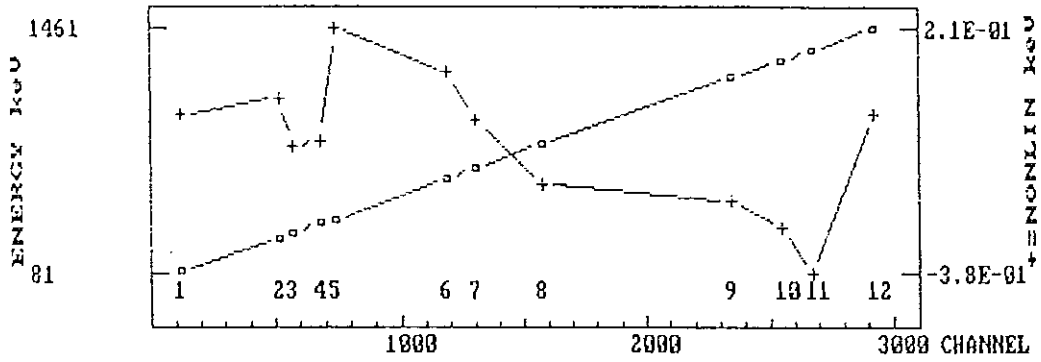

Fig. 4.8 Energy calibration curve obtained by using standard point sources. The plus marks show the deviation of the calibration points from the fitted values. The numbers are just indices to label the lines used in the calibration.

Spectral peaks were identified with specific elements for each sample using the calibration line obtained. Then, shape calibration of the peaks with good statistics in each spectrum was performed in order to carry out the peak fitting process from which the area counts had been calculated. One problem that appeared in the fitting procedure is that the shape of the peaks corresponding to very high counting rates is deformed especially on the high energy side, as a result of pile-up and other electronic effects . γ−ray spectra for the highly active KL sample and for L1S6 and Ld6 are presented in Fig. 4.9, and some examples of the fitting results are shown in Fig. 4.10 for the 1460.8 keV line from ^{40}K, the 1401 keV, 1407 keV, 1765 keV lines of ^{214}Bi, and 351 keV line from ^{214}Pb .

In the Microsampo analysis software, a fit is considered good if the residuals lie within three standard deviation from the fitted curve. The even distribution of the residuals, which is an indication of the accuracy of the fit, about the zero line for the 1460.8 keV line of ^{40}K, for the 1401 keV and 1407 keV lines of ^{214}Bi indicates that the peaks are well fitted. On the

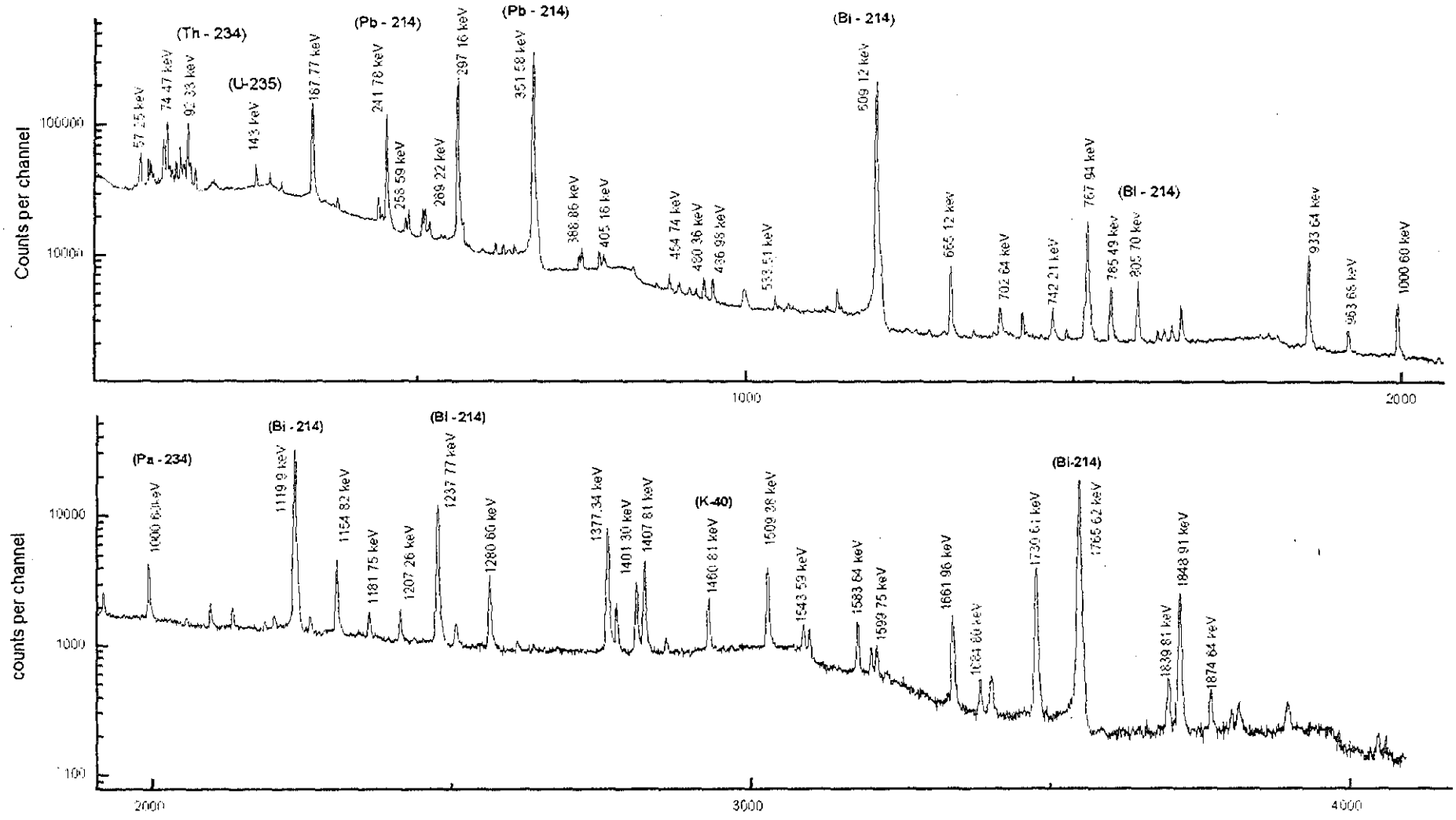

Fig. 4.9a Spectrum of sample KL.

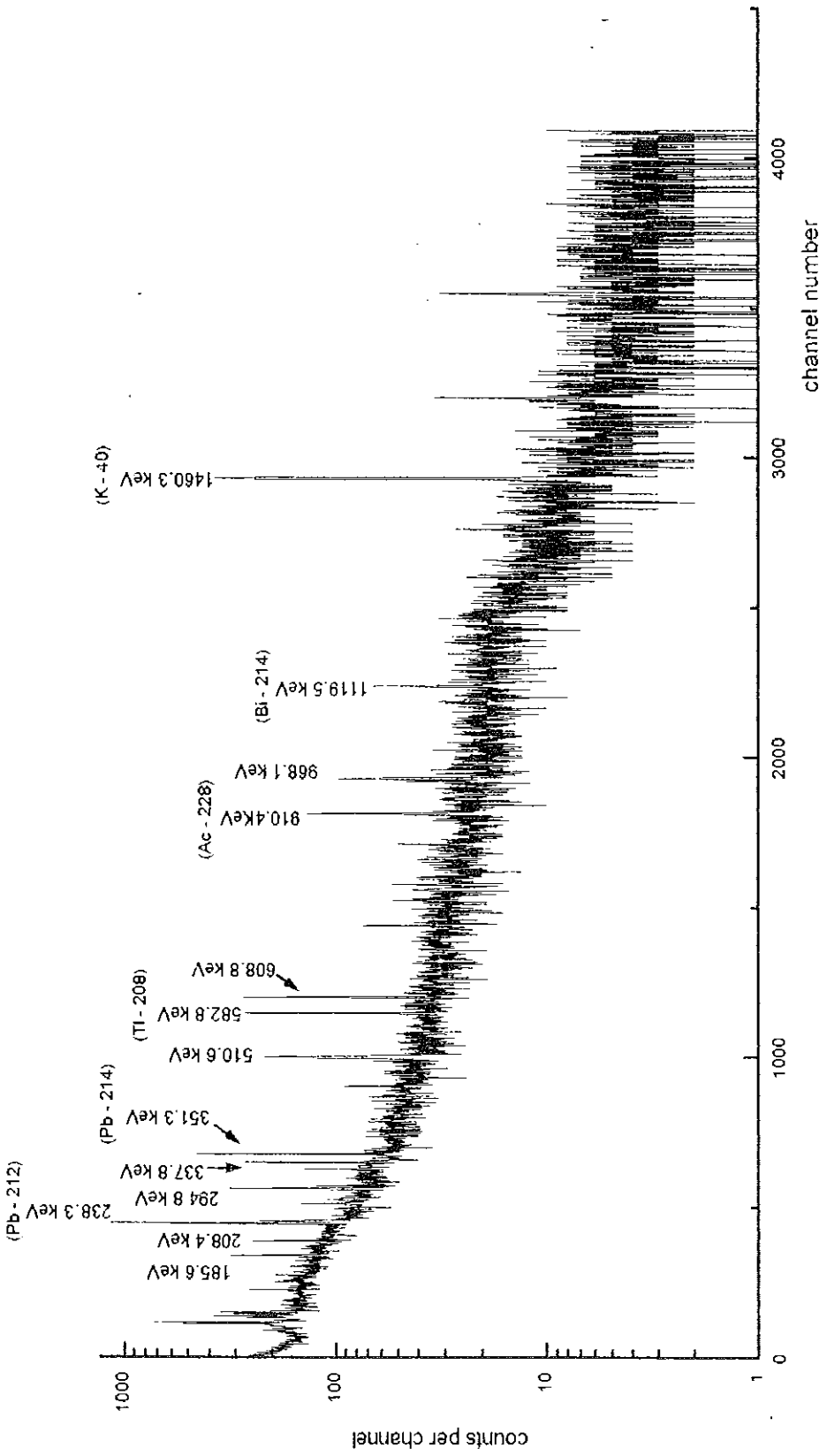

Fig. 4.9c Spectrum of sample LDd.

other hand, the residuals lie mostly above the zero line for the 1765 keV line of ^{214}Bi indicating that the peaks are badly fitted . To improve the fit, peaks at 1765 keV and 1769 keV were inserted manually and fitted together with the 1765 keV line in the case of ^{214}Bi. The results are displayed in Fig. 4.11 and it can be seen that the residuals are more or less evenly scattered showing that the last fit is a good one.

The same thing has been done for peaks with distorted shapes in the spectra of all the samples. This illustrates the fact that one has to take care in handling spectra with high count rates since the activity calculations involve the area counts under each peak which could be erroneous as a result of bad fitting.

To carry out the activity calculations, efficiency calibration was carried out using a soil reference (IAEA-375 soil) obtained from the International Atomic Energy Agency (IAEA). The radionuclides in the soil reference with their corresponding specific activities, reference dates and energies are given in appendix D. The energies and corresponding efficiencies used for the calibration are given in table 4.4.

Table 4.4 Energy and efficiency values used for efficiency calibration

Energy(keV)	176.33	427.88	463.39	600.56	795.84	1,365.16
Efficiency	1.43831E-02	6.83395E-03	6.34437E-03	4.77581-03	3.20679E-03	2.14284E-03

In the calibration process, only the lines above 170 keV were used since for energies below this value no lines with good statistics were obtained. Even if it were possible to find low energy lines with high intensities, it would be preferable not to use them in our case in order

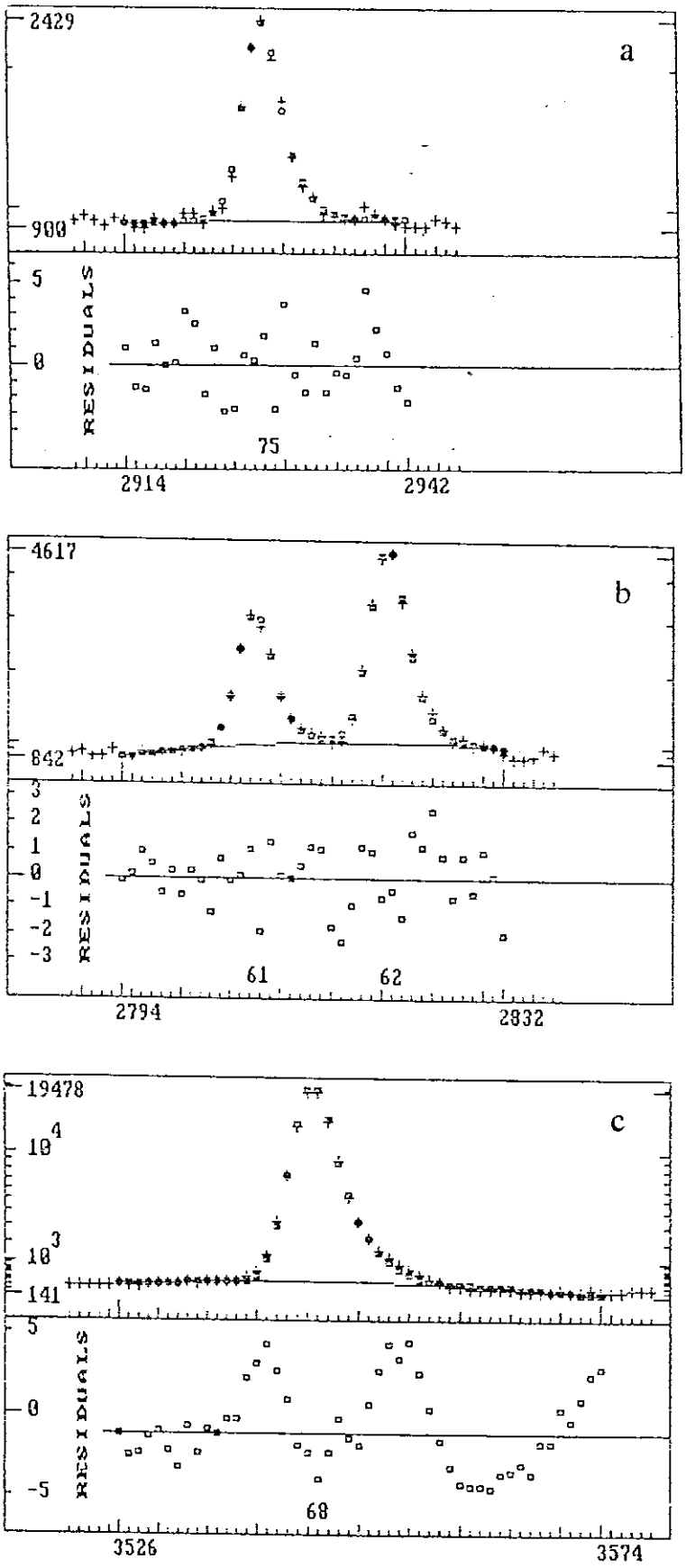

Fig 4.10 Some examples of fitting results from sample KL, a) 1460.8 keV line 0f ^{40}K, b) 1401 keV and 1408 keV lines of ^{214}Bi, c) 1765 keV line of ^{214}Bi.

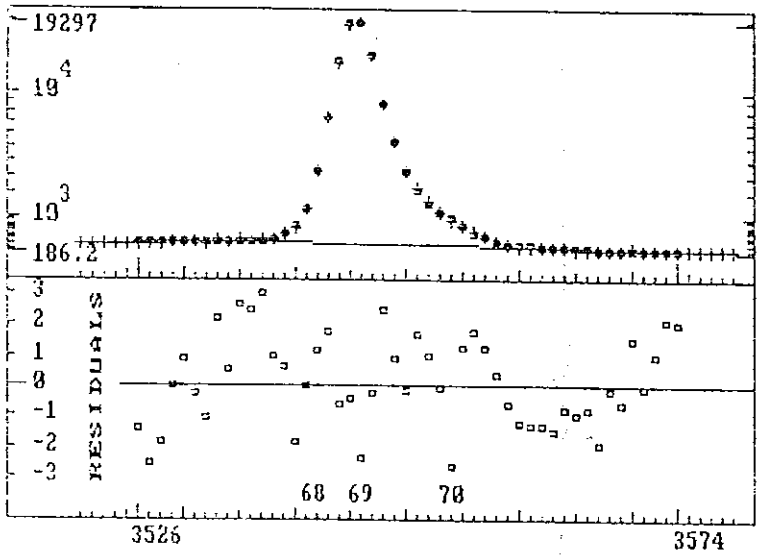

Fig . 4.11 The 1764 keV line of ^{214}Bi after being refitted.

to avoid the difficulties associated with interferences from low energy X-rays. For measurements involving low energies, a low energy germanium detector (LeGe) or a lithium drifted silicon (Si(Li)) detector can be used. The plot of efficiency versus energy is shown in Fig .4.12.

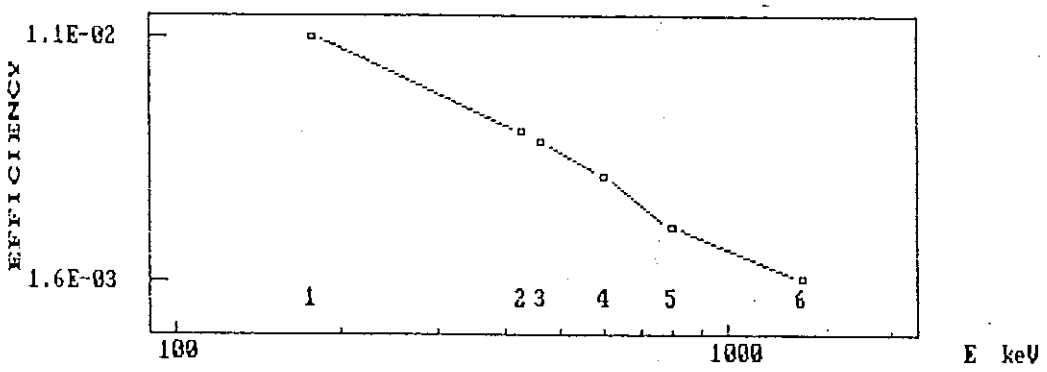

Fig. 4.12 Efficiency calibration curve for the IAEA reference material used as standard source.

4.5 Discussion of Results

Making use of the peak fitting results and the relation between efficiency and energy in accordance with the curve in Fig. 4.12, the software calculated the specific activity for each sample. In the determination of the activity values, the contribution from the external background has been neglected since it contains only the lines from ^{40}K, ^{226}Ra, ^{235}U, and ^{214}Bi with total activity (132.8 Bq) of the order of the uncertainties in the activty values calculated for all samples. The spectrum for the external background is shown in Fig. 4.13. The results are presented in table 4.5 given on the following pages. For sample KL, a report of the analysis as given by MicroSAMPO is presented in appendix E.

On the basis of the total activity for each sample given in table 4.6, the histogram presented in Fig. 4.14 is drawn to give an indication of the radioactivity level of the samples relative to that of sample LD6 which is the least active of all. As can be seen from the figure, sample KL appears to be highly active. The fraction of minerals, KR, separated from the fine grained tantalite concentrate seems moderately active while samples L1S6, L5S1 and KR10 and the clay materials are in general of very low activity.

The lepidolite sample, KL, is a mineral found in pegmatites which are known to contain [PRM] radioactive substances in addition to the rare earth metals. The radionuclides identified with this sample are predominantly from the uranium and thorium series. some elements from the actinium series are also present. Thus, the marked radioactivity of this sample could be attributed to a very high content of uranium and thorium minerals compared to the others.

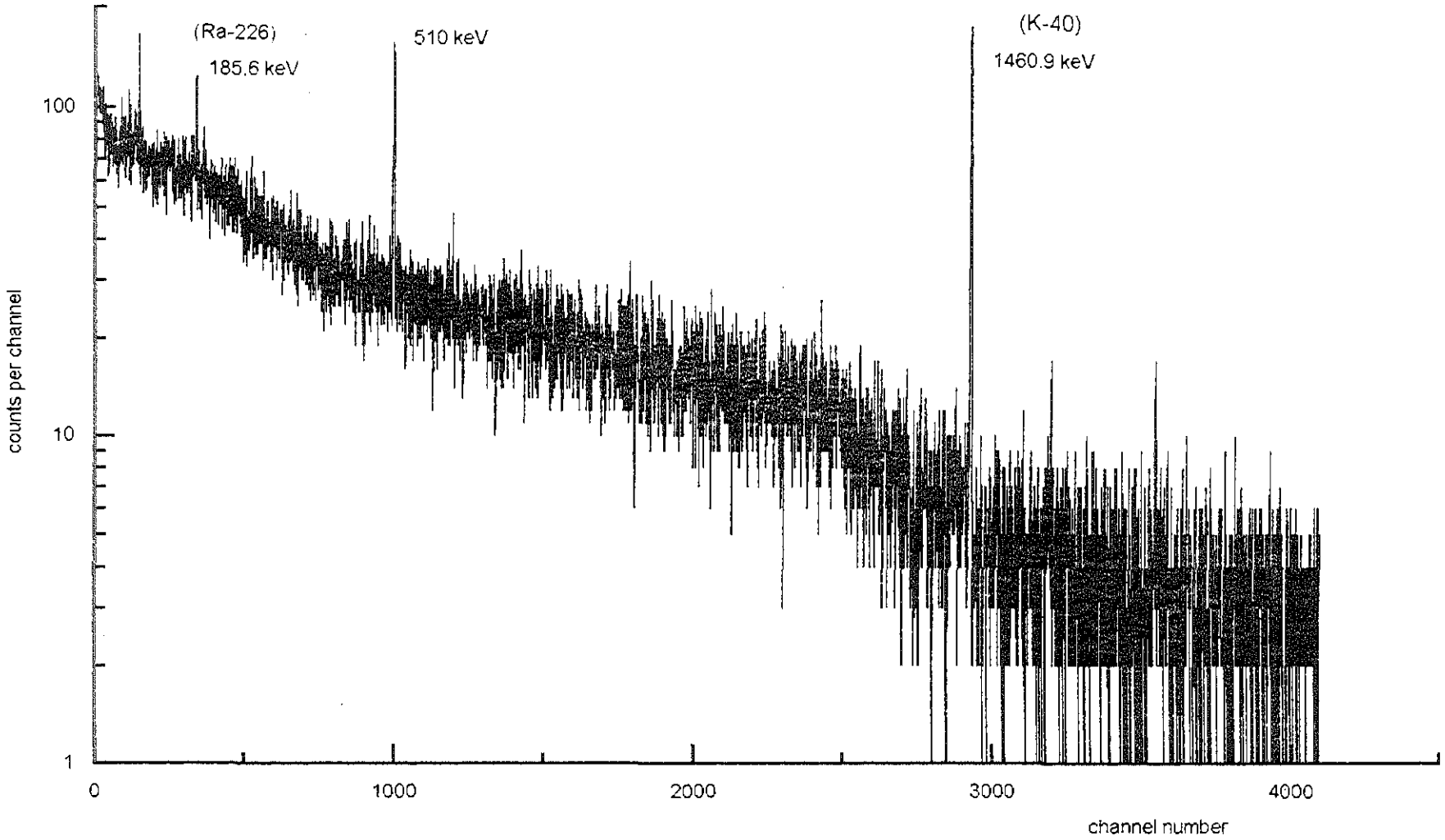

Fig. 4.13 Background spectrum measured with the shielded HpGe detector.

	KL	KR	L1S6	L5S1	KR10	C2	C11	C12
K-40	4358.6 +/- 312.5	506.2 +/- 43.3	2371.7 +/- 164.1	938.3 +/- 67.8	2798.3 +/- 193.6	1045.6 +/- 74.1	1605.3 +/- 113.0	1494.5 +/- 105.2
U-235	2526.4 +/- 213.2	560.6 +/- 50.5	80.6 +/- 9.4	80.48 +/- 14.39	37.70 +/- 4.45	7.5 +/- 1.0	8.0 +/- 1.1	11.5 +/- 1.5
Ra-226U	56414.0 +/- 12037.8	9266.65 +/- 2328.7	1302.03 +/- 151.42	954.8 +/- 357.5	609.0 +/- 71.9	121.4 +/- 15.9	128.5 +/- 17.6	185.7 +/- 23.8
Pb-214U	43475.0 +/- 930.4	9124.2 +/- 227.2	610.1 +/- 42.2	962.4 +/- 43.4	268.4 +/- 14.8	41.0 +/- 2.8	43.0 +/- 2.8	61.2 +/-4.4
Bi-214U	46361.0 +/- 505.3	9261.1 +/- 106.5	591.6 +/- 30.5	935.4 +/- 15.9	257.7 +/- 7.2	41.2 +/- 2.1	41.3 +/- 2.3	65.3 +/- 3.1
Ac-228Th	716.0 +/- 68.3	664.5 +/- 16.8	116.2 +/- 13.9	55.3 +/- 3.1	------	46.0 +/-2.3	55.0 +/- 2.8	94.9 +/- 3.8
Pb-212Th	------	563.1 +/- 44.7	------	53.9 +/- 6.0	------	51.8 +/- 5.6	58.7 +/- 6.4	108.3 +/- 9.2
Tl-208Th	------	173.3 +/- 11.7	------	15.9 +/- 1.5	------	17.4 +/- 1.3	19.2 +/- 1.5	33.4 +/- 2.2
Th-227	2098.3 +/- 226.4	446.2 +/- 49.2	------	6.6 +/- 0.9	------	------	------	------
Bi-211Ac	3293.0 +/- 176.5	562.0 +/- 66.4	------	------	------	------	------	------
Tl-210U	------	------	------	------	------	------	------	------
Ra-224Th	------	------	------	------	------	------	------	2.5 +/- 0.7

Table 4.5 Activity calculation results in Bq/kg

	KRT	C1	C10	C6	C3	C9	CLY	LD6	C7
K-40	1611.7 +/- 114.6	1754.5 +/- 121.9	1763.8 +/- 124.5	1769.0 +/- 124.0	1577.3 +/- 110.1	1566.6 +/- 110.9	1618.0 +/- 114.1	542.5 +/- 39.7	1291.7 +/- 90.6
U-235	25.1 +/- 3.1	8.9 +/- 1.2	10.4 +/- 1.4	10.6 +/- 1.4	8.5 +/- 1.1	9.1 +/- 1.2	13.3 +/- 1.7	5.6 +/- 0.8	6.2 +/- 0.8
Ra-226U	405.9 +/- 49.4	1436.0+/- 188.5	168.5 +/- 22.7	170.5 +/- 22.3	137.8 +/- 17.8	147.6 +/- 20.0	214.3 +/- 27.0	90.0 +/- 12.2	99.4 +/- 13.6
Pb-214U	165.2 +/- 9.6	25.6 +/- 5.9	62.9 +/- 4.3	55.0 +/- 3.8	48.4 +/- 3.1	47.8 +/- 3.6	58.9 +/- 3.5	27.3 +/- 1.9	37.7 +/- 2.6
Bi-214U	157.7 +/- 6.2	49.6 +/- 2.4	56.7 +/- 3.3	53.7 +/- 2.7	44.5 +/- 2.5	48.7 +/- 2.7	56.7 +/- 3.0	25.7 +/- 1.6	37.6 +/- 2.1
Ac-228Th	75.2 +/- 3.8	120.3 +/- 36.3	74.1 +/- 3.7	75.3 +/- 3.3	72.5 +/- 2.8	70.6 +/- 3.4	------	37.9 +/- 1.9	53.0 +/- 2.4
Pb-212Th	75.3 +/- 8.5	121.3 +/- 10.0	85.7 +/- 7.5	83.4 +/- 7.2	74.9 +/- 6.6	69.9 +/- 7.6	------	40.8 +/- 4.4	54.9 +/- 4.9
Tl-208Th	24.5 +/- 1.9	43.4 +/- 2.5	24.8 +/- 1.9	26.0 +/- 1.8	25.4 +/- 1.8	22.9 +/- 1.8	------	43.0 +/- 3.3	19.9 +/- 1.5
Th-227	------	------	------	------	------	------	------	------	------
Bi-211Ac	------	64.8 +/- 19.7	------	------	------	------	------	------	------
Tl-210U	------	6.1 +/- 0.7	------	------	------	------	------	------	------
Ra-224Th	------	66.4 +/- 23.4	------	------	------	------	------	------	------

Table 4.5 Cont.

Table 4.6 Total activity in Bq / kg of samples as calculated by MicroSAMPO software. The last column contains the activity of the samples normalised to that of sample LD6

	pCi/kg	μCi/kg	Bq/kg	Rel. activity
KL	4.372E + 06	4.372E + 00	16.18E + 04	206.3
KR	8.565E + 05	8.565E - 01	3.17E + 04	40.4
L1S6	1.371E + 05	1.371E - 01	5.07E + 03	6.5
L5S1	1.12E + 05	1.12E - 01	4.14E + 03	5.3
KR10	1.075E + 05	1.075E - 01	3.98E + 03	5.1
KRT	6.867E + 04	6.867E - 02	2.54E + 03	3.2
C1	6.499E + 04	6.499E - 02	2.40E + 03	3.1
C10	6.072E + 04	6.072E - 02	2.25E + 03	2.9
C12	5.5648E + 04	5.5648E - 02	2.06E + 03	2.6
C3	5.376E + 04	5.376E - 02	1.99E + 03	2.5
C9	5.36E + 04	5.36E - 02	1.98E + 03	2.5
CLY	5.3E + 04	5.3E - 02	1.96E + 03	2.5
C11	5.29425E + 04	5.294E - 02	1.96E + 03	2.5
C6	4.54725 + 04	4.547E - 02	1.68E + 03	2.1
C7	4.324E + 04	4.324E - 02	1.60E + 03	2
C2	3.708E + 04	3.708E -02	1.37E + 03	1.7
LD6	2.1195E + 04	2.119E - 02	0.78E + 03	1

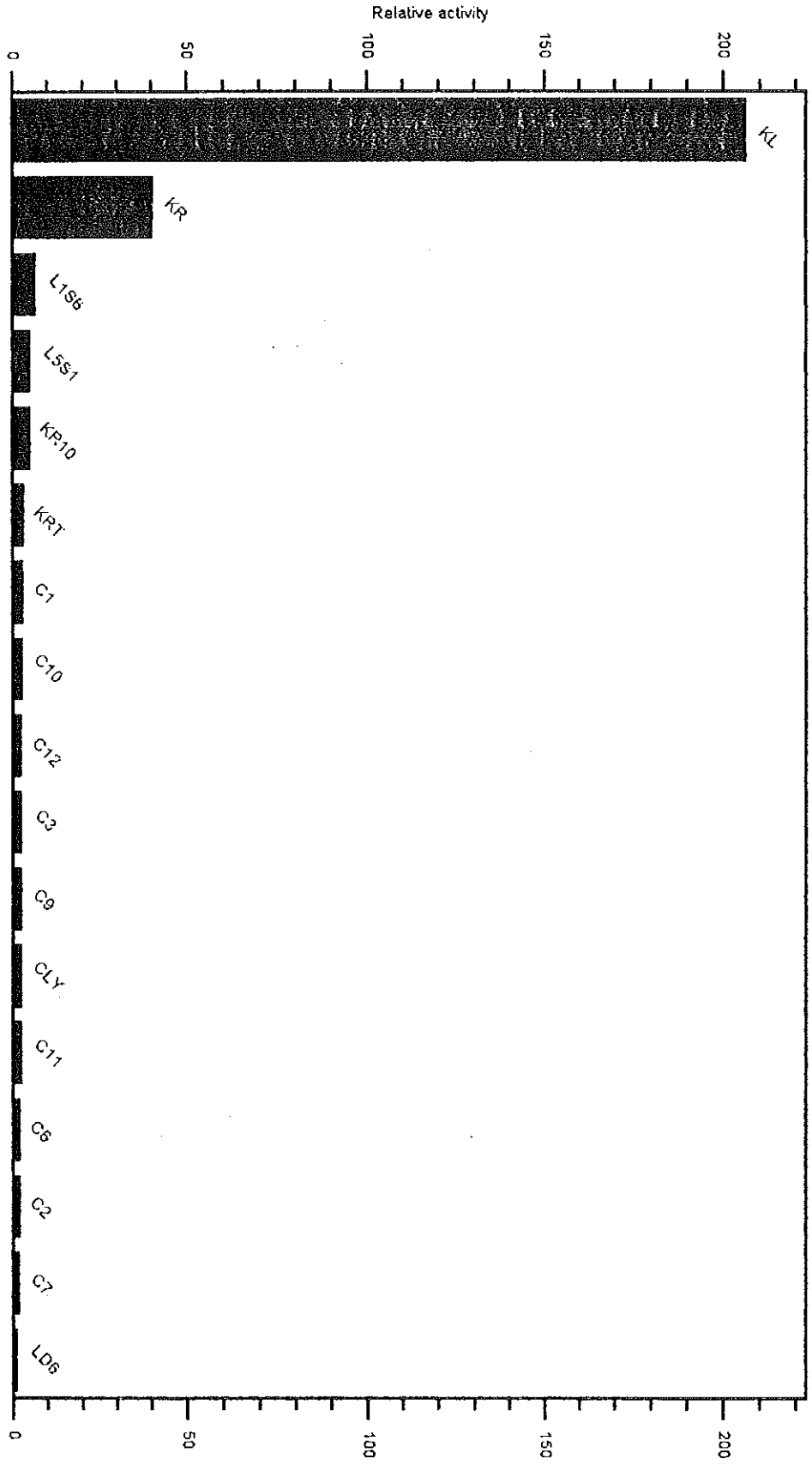

Fig. 4.14 A histogram showing the relative distribution of radioactivity of the seventeen samples.

The sample KR shows a high level of radioactivity next to KL. The radionuclides associated with this sample are also mainly from the uranium and thorium series. This implies that the tantalite mineral has a high concentration of uranium and thorium.

The deluvium samples L1S6, L5S1 and KR10 are more active than the clay materials probably because they are usually found covering the weathered pegmatites as irregular (in thickness) layers. These samples also contain radionuclides mainly from the uranium and thorium series .

Even though the clay materials were taken from the initial tantalite containing ores stocked for treatment at the Kenticha pilot plant, they are in general of very low activity may be because the concentration of minerals, before the treatment, with which radioisotopes from the uranium and thorium series are associated is very small. In this case also, the radioisotopes identified are from the uranium and thorium series. To see other radioisotopes found in the various samples, one can refer to table 4.5.

Looking at the concentrations of ^{226}Ra, ^{214}Pb and ^{214}Bi, it is apparent that the values obtained for samples KR and L5S1 are comparable within the uncertainties indicated. This suggests that, for these samples, equilibrium has somewhat been reached between parent and daughters. In the case of sample KL, the concentrations of ^{226}Ra, ^{214}Pb and ^{214}Bi are fairly close to each other but are not within overlapping uncertainties. This implies that, for this sample, the waiting time should have been longer to establish equilibrium conditions. For the above mentioned samples, the determination of ^{226}Ra (186.2 keV) in the presence of the peak at 185.7 keV from ^{235}U has been possible since the concentration of ^{235}U was calculated using not only the 185.7 keV line but also the lines at 163.3 keV and 205.3 keV.

For the remaining samples, the concentration ^{235}U was computed only from the peak at 185.72 keV for the lines at 163.33 keV and 205.31 keV were not found in the spectra as a result of the weak intensities involved. The concentration calculated for ^{226}Ra is thus quite larger than those obtained for ^{214}Pb and ^{214}Bi apparently due to the interference from the 185.7 keV line of ^{235}U. A closer look at the values of ^{226}Ra and ^{235}U indicates that the concentration of ^{226}Ra becomes comparable to those of ^{214}Pb and ^{214}Bi if 10 times the concentration of ^{235}U is subtracted from the results obtained for ^{226}Ra as shown in table 4.7. In the light of what has been discussed above, the concentration of ^{238}U from the values obtained for ^{226}Ra, ^{214}Pb and ^{214}Bi would be as given in the last column of table 4.7.

For samples KL and L1S6, the software was not able to identify the peaks from ^{212}Pb and ^{208}Tl making the determination of ^{232}Th difficult. In samples KR10 and CLY, the lines of ^{228}Ac and ^{212}Pb have not been found at all may be due to low intensity problems or they do not contain any radioisotopes from the thorium series. For the rest of the samples, the values obtained for ^{228}Ac and ^{212}Pb are found to be comparable while the concentration of ^{208}Tl appears to be about three times smaller for the remaining samples. In this case also, either the efficiency values for its lines are bigger than they should be or it is a problem of equilibrium. However, if we took into account the missing factor and make a correction for the activity of ^{208}Tl in order to estimate the of concentration of ^{232}Th, the result would be as shown in the last column of table 4.8.

Table 4.7 Activity values in Bq / kg of ^{226}Ra, ^{214}Pb, and ^{214}Bi used for the determination of ^{238}U

	^{226}Ra	^{214}Pb	^{214}Bi	^{238}U
KL	56414.0 +/- 12037.6	43475.0 +/- 930.3	46361.0 +/- 505.3	45718.1+/- 899.7
KR	9266.7 +/- 2328.7	9124.2 +/- 227.2	9261.1 +/- 106.5	9236.4 +/- 37.2
L1S6	496.2 +/- 178.1	610.1 +/- 42.2	591.6 +/- 30.5	596.0 +/- 11.6
L5S1	954.8 +/- 357.5	962.4 +/- 43.4	935.4 +/- 15.9	938.6 +/- 6.2
KR10	232.0 +/- 84.6	268.4 +/- 14.8	257.7 +/- 7.2	271.8 +/- 9.3
C2	46.3 +/- 16.0	41.0 +/- 2.8	41.2 +/- 2.1	41.2 +/- 0.4
C11	49.0 +/- 17.6	43.0 +/- 2.8	41.3 +/- 2.3	42.0 +/- 0.8
C12	70.8 +/- 23.9	61.2 +/- 4.3	65.3 +/- 3.1	64.0 +/- 1.5
KRT	154.7 +/- 58.1	165.2 +/- 9.6	157.7 +/- 6.2	159.9 +/- 2.4
C1	—	25.6 +/- 5.9	49.6 +/- 2.4	—
C10	64.2 +/- 26.7	62.9 +/- 4.3	56.7 +/- 3.3	59.0 +/- 2.1
C6	65.0 +/- 26.2	55.0 +/- 3.8	53.7 +/- 2.7	54.2 +/- 0.8
C3	52.5 +/- 21.0	48.4 +/- 3.1	44.5 +/- 2.5	46.1 +/- 1.4
C9	56.3 +/- 23.5	47.8 +/- 3.4	48.7 +/- 2.7	48.4 +/- 0.7
CLY	81.7 +/- 31.8	58.9 +/- 3.5	56.7 +/- 3.0	57.7 +/- 1.4
LD6	34.3 +/- 12.2	27.3 +/- 1.9	25.7 +/- 1.6	26.5 +/- 0.8
C7	37.9 +/- 16.0	37.6 +/- 2.6	37.6 +/- 2.1	37.6 +/- 0.03

Table 4.8 Activity values in Bq / kg of ^{228}Ac, ^{212}Pb, and ^{208}Tl used for determination of ^{232}Th

	^{228}Ac	^{212}Pb	^{208}Tl	^{232}Th
KL	716.0 +/- 68.3	—	—	—
KR	664.5 +/- 16.8	563.1 +/- 44.7	519.9 +/- 34.0	628.8 +/- 58.7
L1S6	116.2 +/- 13.9	—	—	—
L5S1	55.2 +/- 3.1	53.9 +/- 6.0	47.6 +/- 4.5	53.0 +/- 2.5
KR10	—	—	—	—
C2	46.0 +/- 2.3	51.8 +/- 5.6	52.3 +/- 4.0	48.0 +/- 2.9
C11	55.0 +/- 2.8	58.7 +/- 6.4	57.5 +/- 4.5	56.1 +/- 1.0
C12	94.9 +/- 3.5	108.3 +/- 8.7	99.8 +/- 6.1	96.8 +/- 2.8
KRT	75.2 +/- 3.8	75.3 +/- 8.5	73.4 +/- 5.8	74.8 +/- 0.6
C1	120.3 +/- 3.6	121.3 +/- 10.0	130.3 +/- 7.5	122.1 +/- 2.6
C10	74.1 +/- 3.7	85.7 +/- 7.5	74.3 +/- 5.8	75.8 +/- 2.3
C6	75.3 +/- 3.3	83.4 +/- 7.2	77.9 +/- 5.3	77.0 +/- 2.0
C3	72.5 +/- 2.8	74.9 +/- 6.6	76.2 +/- 5.4	73.4 +/- 1.1
C9	70.6 +/- 3.4	69.9 +/- 7.6	68.6 +/- 5.4	70.0 +/- 0.6
CLY	—	—	—	—
LD6	37.9 +/- 1.9	40.8 +/- 4.4	43.0 +/- 3.3	39.4 +/- 1.5
C7	52.3 +/- 2.4	54.9 +/- 4.9	59.8 +/- 4.4	54.6 +/- 1.9

4.6 Conclusion

An attempt has been made to measure the natural radioactivity of samples brought from the Kenticha tantalite processing area and estimate the uranium and thorium concentration in the various samples. For the analysis of the spectra measured, a soil reference material was employed as standard. However, the low energy region of the various spectra was not considered due to lack of enough calibration points for the standard source used was not a newly prepared one. Even if it were possible to find low energy lines with good statistics, it would be advisable to use, if available, a Si(Li) or LeGe detector in order to obtain reliable information from the low energy region where X–rays happen to interfere with γ–rays.

As the results obtained in this work indicate, few of the samples exhibit an enhanced level of radioactivity because of their relatively high concentration of uranium and thorium. This is particularly apparent if comparison is made between the activities of samples KL & KR and the other ones. A higher level of natural radiation at some spots in the Kenticha mining area is evident. Though such practice is known to result in an increased radiation health hazard, quantitative measurements and dose assessments have to be carried out in this area to give a full picture of the radiation risk incurred by the miners working there. Public exposure to radiation from the natural environment is also suggested to be carried out.

Concerning the determination of uranium and thorium content of the samples, one should keep the samples, before measurement, in a container tightly sealed (to keep ^{222}Rn and ^{220}Rn, whcich are gases, from escaping) for a sufficiently long time to make sure that equilibrium between parent and daughter nuclides is attained. In addition, long measuring times for samples of low activity and a good standard source for efficiency calibration are necessary to make more accurate measurements.

Outlook

It is essential to note that this work is just the beginning in the direction of applied nuclear physics. There should be reasons why a factor of about ten for the ^{235}U series and three for the ^{232}Th series appear in the determination of their concentrations. This means, a systematic study of the natural radioactivity around the Adola mining region must be carried out in the future to make conclusive statements about the concentrations of ^{238}U and ^{232}Th.

References

[ADW] Anderson, D. W., Absorption of ionising radiation, University park press, Baltimore (1984)

[BGR] Boswell, G.G., & Fairs, Radioisotope Laboratory Technique, Butterworth & Co. Ltd., Boston(1981)

[CNP] Canberra Nuclear Products Group, edition nine.

[CPN] Cooper, P. N., Introduction to nuclear radiation detectors, Cambridge University press, New York (1986).

[DHG] Debertin, K., Helmer, R. G., Gamma- and X-ray Spectrometry with Semiconductor Detectors, North Holland, Amsterdam (1988).

[EAF] Efimov, A. F. et al., Rare metals of Kenticha and other pegmatite fields of the Adola area (internal report of EMRDC), Ministry of Mines and Energy, Addis ababa (1985)

[EIM] Eisenbud, M., Environmental radioactivity, McGraw-Hill, New York (1963).

[HKH] Haller, E. E., Kraner, H.W., Higinbotham, W. A., (Eds) Nuclear Radiation Detector Materials, (Symp. Proc., Boston (1982), Massachusetts, U. S. A.), Vol. 16, Materials Research Society, North Holland, Amsterdam (1983).

[IAEA1] International Atomic Energy Agency, Application of dose limitation system to the mining and milling of radioactive ores (Safety series no. 82, IAEA safety guides), IAEA, Vienna (1987).

[IAEA2] International Atomic Energy Agency, Environmental contamination by radioactive materials (Proc. Semi. Vienna (1969)), IAEA, Vienna (1969).

[IAEA3] International Atomic Energy Agency, Measurement of radionuclides in food and the environment (Technical reports series no.295), IAEA, Vienna (1989).

[IAEA4] International Atomic Energy Agency, Methods of low level counting and spectrometry (Proc. Symp. Berlin (West),1981), IAEA, Vienna (1981).

[IAEA5] International Atomic Energy Agency, Population dose evaluation and standards for man and his environment (Proc. Semi. Portoroz (1974)), IAEA, Vienna (1974).

[IAEA6] International Atomic Energy Agency, Radiation protection of workers in the mining and milling of radioactive ores (Safety series no. 26, IAEA safety standards), IAEA, Vienna (1983).

[IAEA7] International Atomic Energy Agency, Rapid methods for measuring radioactivity in the environment (Proc. Symp. Neuherberg(1971)), IAEA, Vienna (1971).

[IAEA8] International Atomic Energy Agency, Uranium deposits in volcanic rocks, (Proc. Tech. Comm. Meeting, El Paso(1984)), IAEA, Vienna (1985).

[IAEA9] International Atomic Energy Agency, Nuclear techniques in the exploration and exploitation of energy and mineral resources (Proc. Symp. Vienna (1990)), IAEA, Vienna (1991).

[IAEA10] International Atomic Energy Agency, Application of isotopes and radiation in conservation of the environment (Proc. Symp. Karlsruhe(1992)), IAEA, Vienna(1992).

[IAEA11] International Atomic Energy Agency, Radiation a fact of life, IAEA, Vienna (Sept. 1979).

[IAR] International commission on radiological protection, Annals of the ICRP, ICRP publication 60, Pergamon Press, Oxford(1991).

[KGF] Knoll, G. F., Radiation detection and measurement, 2nd edition, Wiley, New York (1989).

[PRM] Pearl, R. M. Rocks and minirals, Rev. edition, Barnes & Noble, New York (1956).

[PWJ] Price, W.J., Nuclear radiation detectors, 2nd ed., McGraw-Hill, New York (1964)

[RAK] Rankama, K., Isotope geology, p. 195, McGraw Hill, New York (1954).

[SJR] Shapiro, J., Radiation protection, Harvard University press, Cambridge, Massachusetts (1972).

[SKA] Siegbahn, K. (Ed.), Alpha, beta and gamma ray spectroscopy, chap. 5, pp. 283-295, North Holland, Amsterdam (1965).

[SRM] Singru, R.M., Introduction to experimental nuclear physics, Wiley Eastern, New Delhi (1972).

[USB] United Nations Scientific Comitte on the effects of atomic radiation: Sources, Effects and Risks of ionising radiation, UNSCEAR, United Nations, New York (1988).

[USE] United Nations Scientific comitte on the effcts of atomic radiation, Ionising Radiation: Sources and biological effects, UNSCEAR, United Nations, New York(1988).

he three naturally occuring radionuclide series

d for sample collection

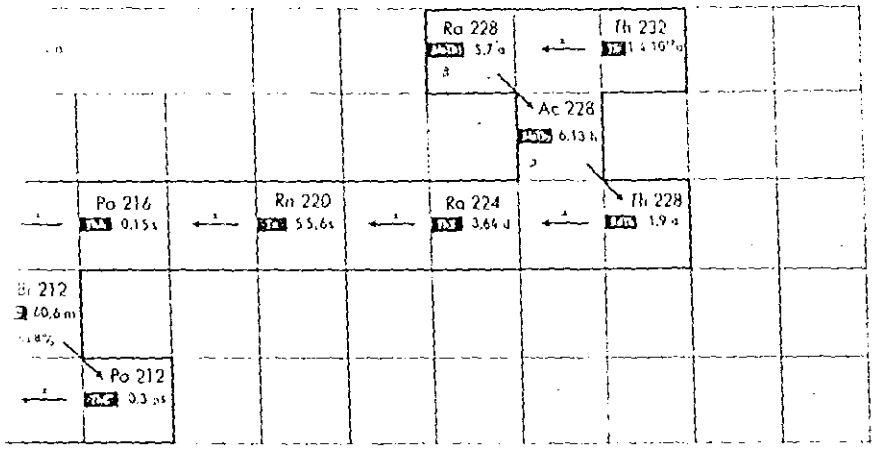

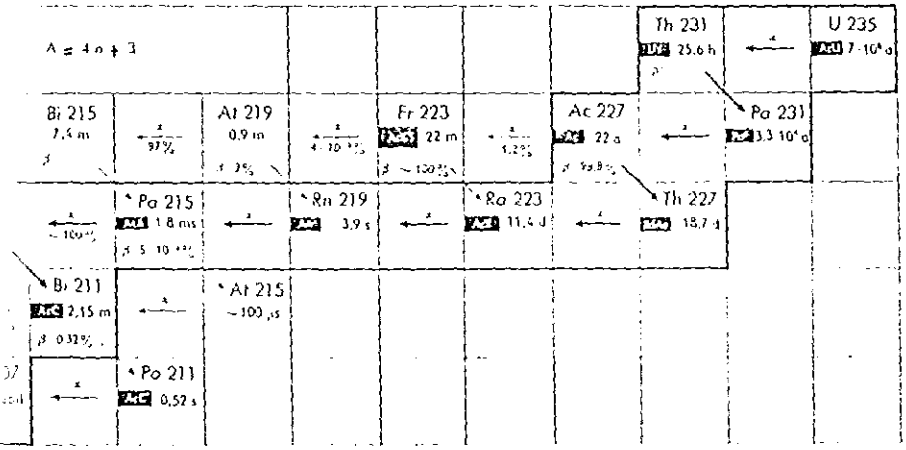

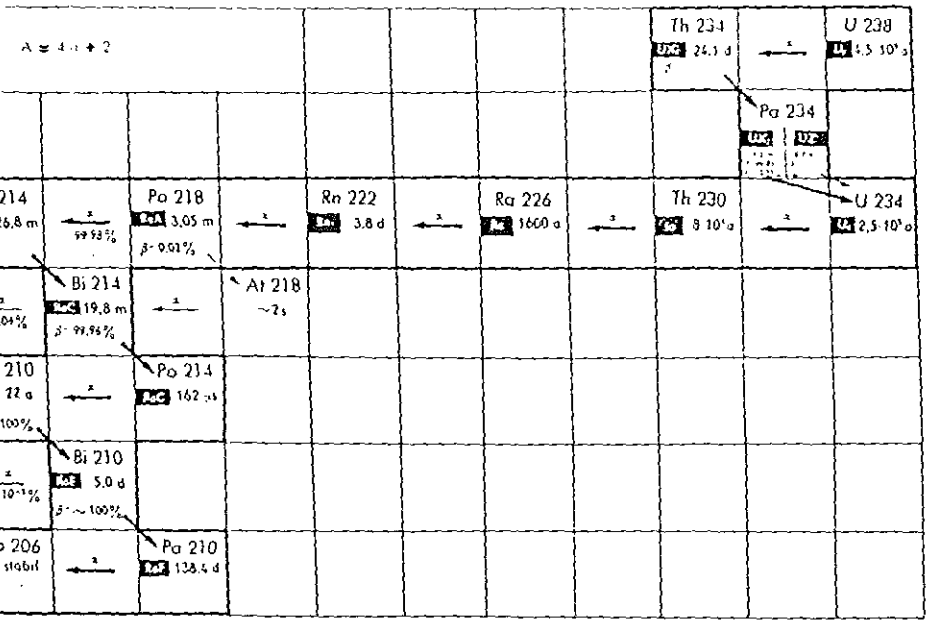

2.0 kg)

10 mm

10 min

0.50 kg

10 min

50 kg)

Appendix C. The operational procedure of the MicroSAMPO software

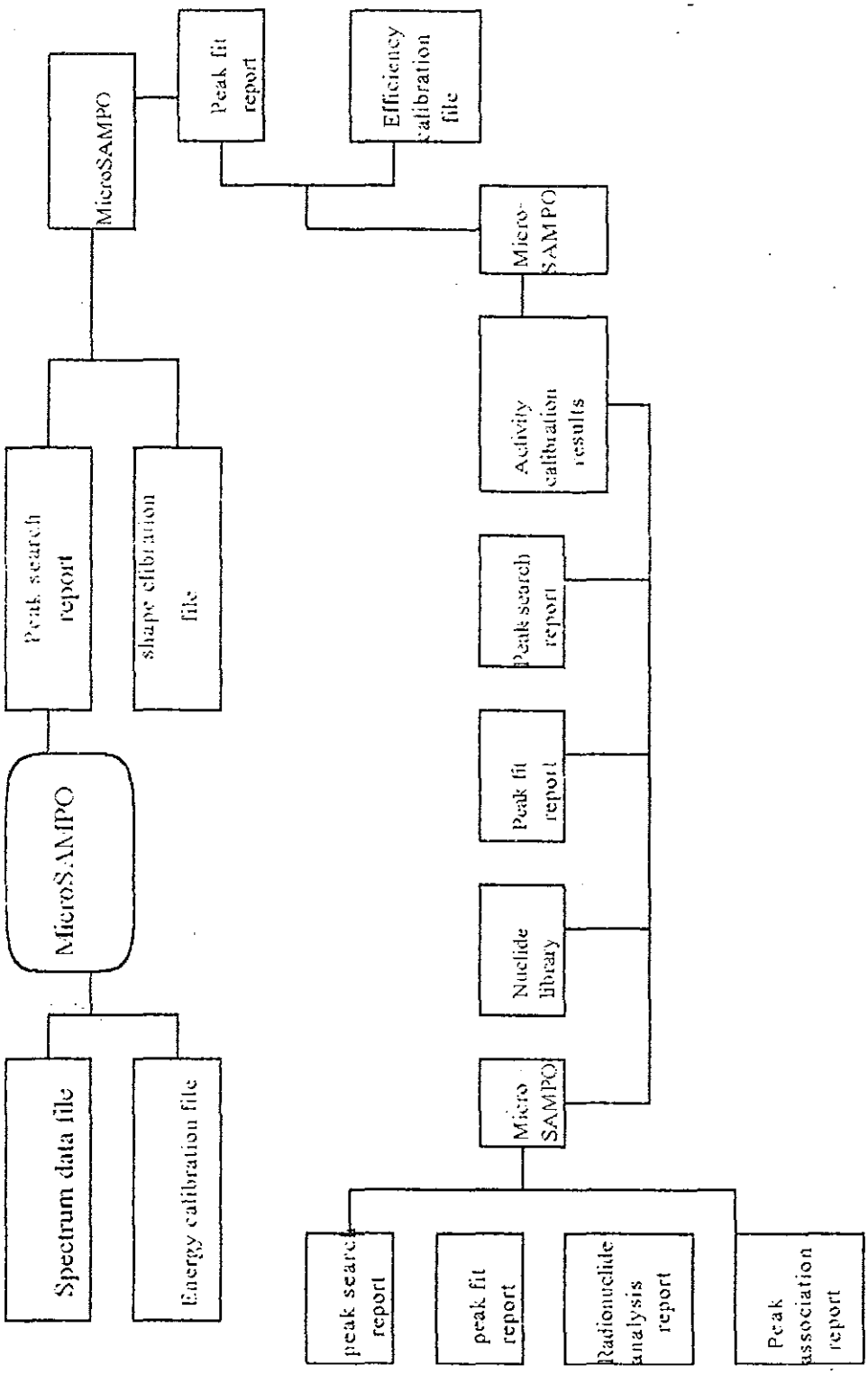

Appendix D. The equation used by MicroSAMPO for efficiency calibration

The equation used by the MicroSAMPO software for efficiency calibration is

$$f(E) = \frac{(\ln 2) N \; t_m}{t_l \; b A \; 2^{(\frac{-t_w}{T})} T \; (1 - 2^{(\frac{-t_m}{T})})}$$

where N = the γ peak area for the peak at energy E,

A = the activity (decays / sec) of the calibration nuclide at the time t_w prior to the start of counting,

t_m = the real measuring time,

t_l = the live measuring time,

T = the half-life of the calibration nuclide,

b = the branching ratio, that is the average no. of γ quanta with energy E emitted per one decay.

The uncertainty of the detector efficiency (in %) is calculated as

$$df = \text{sqrt}\ (\ (dA)^2 + (dN)^2\ )$$

where dA is relative uncertainty of the calibration source activity (in %), dN is relative uncertainty of the gamma peak area (in %) as given by MicroSAMPO. In principle, the uncertainties of the branching ratio, half-life, and measuring times should also be included in the expression of df, but the values are not easily available and their effect is usually rather small.

Between the points in the calibration curve, the efficiency values for other energies are calculated by log-log interpolation. Below the first calibration point and above the last one the efficiency values are calculated by log-log extrapolation from the two closest points.

The sources used in this work for efficiency calibration, their energies, and activity values are given in the table shown below:

Source	Energy in keV	Activity in Bq / kg	Confidence interval in Bq / kg
^{125}Sb	176.33 427.88 463.34 600.56	77	74–79
^{134}Cs	795.84 1365.16	463	454–472

The values of the activities given in the table are the best estimates as of April 1994. The values has been taken from the reference sheet (1994-08-12), with 31 December 1991 as a reference date, and supplied by the International Atomic Energy Agency, Vienna, Austria:

REFERENCE SHEET

IAEA–375

Th, U and RADIONUCLIDES

IN SOIL

ANALYTICAL QUALITY CONTROL SERVICES

INTERNATIONAL ATOMIC ENERGY AGENCY

Appendix E. continued

	80	2774.43	1385.03	4.2403E+03	2.7	5.9063E+03	7.9283E+01	7.3	2.2
m	81	2807.40	1401.30	9.1049E+03	1.7	6.9279E+03	1.5044E+02	7.0	2.1
M	82	2820.57	1407.81	1.6087E+04	1.1	7.0765E+03	3.6672E+02	6.9	2.1
	83	2856.70	1425.64	1.2313E+03	9.6	6.4665E+03	2.0608E+01	11.8	.9
	84	2927.95	1460.81	6.8493E+03	2.3	6.9643E+03	1.1674E+02	7.2	1.1
	85	3026.37	1509.38	1.4876E+04	1.2	7.6525E+03	2.5983E+02	6.9	1.3
m	86	3086.10	1538.86	2.8253E+03	3.6	6.9430E+03	5.0065E+01	7.7	1.1
M	87	3095.68	1543.59	2.3510E+03	4.0	6.4916E+03	4.1756E+01	7.9	1.1
	88	3176.83	1583.64	4.6050E+03	2.7	4.7634E+03	8.3370E+01	7.3	.7
m	89	3200.19	1595.17	1.9191E+03	3.7	4.3948E+03	3.4770E+01	7.7	.9
M	90	3209.46	1599.75	2.2207E+03	3.3	4.2892E+03	4.0509E+01	7.6	.9
	91	3335.50	1661.96	6.7344E+03	1.7	2.8884E+03	1.2640E+02	7.0	1.9
	92	3381.78	1684.80	1.3495E+03	5.6	2.3357E+03	2.5589E+01	8.8	1.4
	93	3400.30	1693.94	1.3716E+03	6.4	2.6656E+03	2.6113E+01	9.3	3.3
	94	3471.59	1730.61	1.9112E+04	.9	2.5693E+03	3.6974E+02	6.8	1.5
	95	3545.56	1765.64	9.6444E+04	.3	3.1351E+03	1.8039E+03	6.8	11.8
	96	3695.83	1839.81	1.7593E+03	4.4	1.8198E+03	3.5637E+01	8.1	1.7
	97	3714.27	1848.91	1.2143E+04	1.1	1.9831E+03	2.4689E+02	6.9	1.6
	98	3766.40	1874.64	1.1851E+03	6.0	1.8055E+03	2.4338E+01	9.1	.8

Flags: m = a peak in a multiplet, M = last peak in a multiplet, ? = bad fit

******** RADIONUCLIDE ANALYSIS REPORT ********

number	nuclide	conf.value	Activity (pCi/kg) measured		decay corrected	saturation
1	PB-212TH	.9918	1.776E+02	+- 19.31%	1.776E+02	0.000E+00
2	PB-214U	.9068	1.175E+06	+- 2.14%	1.175E+06	0.000E+00
3	BI-211AC	.9710	8.900E+04	+- 5.36%	8.900E+04	0.000E+00
4	BI-214U	.6930	1.257E+06	+- 1.14%	1.257E+06	0.000E+00
5	ra-226u	.9886	1.527E+06	+- 20.83%	1.527E+06	0.000E+00
6	TH-227	.6877	5.672E+04	+- 10.79%	5.672E+04	0.000E+00
7	U-235	.9914	6.855E+04	+- 8.41%	6.855E+04	0.000E+00
		totals:	4.173E+06		4.173E+06	0.000E+00

Flags: C = check: nuclide is a part of an underdetermined solution

These peaks were not identified:

number	channel	energy	peak intensity (gps)
4	438.4	235.76	6.294E+01 +- 19.33%
13	563.4	297.16	7.868E+01 +- 16.50%
15	629.3	329.56	2.423E+01 +- 10.07%
16	646.3	337.94	1.947E+01 +- 10.61%
18	744.9	386.76	2.672E+01 +- 9.31%
23	897.7	461.89	1.894E+01 +- 19.46%
24	913.5	469.66	1.304E+01 +- 20.34%
25	922.9	474.31	1.241E+01 +- 20.02%
29	1137.8	580.00	3.887E+01 +- 8.34%
38	1627.6	820.74	1.876E+01 +- 8.58%
39	1637.6	825.68	2.039E+01 +- 7.77%
43	1918.1	963.68	4.348E+01 +- 5.74%
44	1993.2	1000.60	1.341E+02 +- 4.14%
45	2096.7	1051.56	4.176E+01 +- 6.26%
46	2133.3	1069.56	3.158E+01 +- 7.28%
48	2262.7	1133.24	2.486E+01 +- 8.43%
50	2361.3	1181.75	4.435E+01 +- 7.08%
53	2506.2	1253.02	3.087E+01 +- 8.50%

Appendix E. continued

PEAK ASSOCIATION REPORT

nuclide	peak number	peak channel	peak energy	peak usage
PB-212TH	27	413.55	238.28	100.00%
PB-214U	29	450.69	241.79	103.14%
	30	484.82	258.59	101.94%
	33	517.09	274.48	100.48%
	35	558.71	294.87	95.97%
	38	616.93	323.49	9.29%
	41	673.96	351.56	108.29%
	50	935.23	480.36	109.27%
	51	948.68	486.98	127.47%
	52	1043.28	533.51	103.13%
	60	1555.95	785.49	108.93%
	65	1663.92	838.61	81.38%
BI-211AC	41	673.96	351.56	108.29%
	45	782.31	405.15	119.84%
	64	1649.74	831.63	85.91%
BI-214U	43	749.18	388.36	120.60%
	46	883.14	454.75	145.07%
	54	1196.99	609.11	106.48%
	55	1311.05	665.12	109.18%
	56	1387.37	702.64	105.94%
	57	1421.95	719.58	106.15%
	58	1467.88	742.21	8.17%
	59	1520.18	767.91	95.50%
	60	1555.95	785.49	108.93%
	61	1597.05	805.70	91.62%
	66	1857.05	933.64	97.75%
	71	2235.58	1119.89	95.47%
	73	2306.56	1154.82	99.41%
	75	2413.18	1207.26	106.99%
	76	2475.22	1237.77	98.28%
	78	2562.33	1280.60	104.60%
	79	2758.85	1377.34	97.84%
	80	2774.43	1385.03	114.81%
ra-226u	24	336.79	185.73	100.00%
TH-227	29	479.57	256.01	100.42%
	31	506.40	269.22	.07%
	32	510.04	271.00	.06%
	44	775.43	401.77	.18%
U-235	23	290.78	163.08	109.59%
	24	336.79	185.73	100.00%
	25	376.32	205.19	89.31%

Flags: C = check; nuclide is a part of an underdetermined solution